# NASA Contractor Report 172456

NASA-CR-172456
19850007376

# Supersonic Nonlinear Potential Flow Analysis — Interim Report

**M. J. Siclari**

**Grumman Aerospace Corporation**
**Bethpage, NY 11714**

**Contract NAS1-16758**
**August 1984**



National Aeronautics and
Space Administration

**Langley Research Center**
Hampton, Virginia 23665

REPORT RE-690

# SUPERSONIC NONLINEAR POTENTIAL FLOW ANALYSIS - INTERIM REPORT

AUGUST 1984

prepared by

Michael J. Siclari
Fluid Mechanics Directorate

Research and Development Center
Grumman Aerospace Corporation
Bethpage, New YOrk 11714

Interim Final Report on
Contract NAS1-16758

prepared for

National Aeronautics and Space Administration
Hampton, VA 23665

Approved by: Richard A. Scheuing
Richard A. Scheuing, V.P.
Director, R&D Center

CONTENTS

ILLUSTRATIONS

ILLUSTRATIONS (continued)

# 1. INTRODUCTION

The numerical solution of supersonic flow problems using the full potential equation has become an attractive and promising alternative to solving either Euler equations or the linearized potential flow equations. The full potential equation retains most of the nonlinear features of the flow field, such as shocks, that the linearized potential, e.g., the more popular linear panel methods, inherently neglect, while having the simplicity of a single variable irrotational solution. Primitive variables, entropy singularities, and CFL stability conditions tend to complicate Euler equation solvers[1].

The current approach to supersonic flows was first established by Grossman[2] for the conical flow problem using a nonconservative form of the potential equation. The conical flow problem reduces the full potential equation to an equation which in the crossflow plane (i.e., transverse plane normal to conical rays) contains all of the salient features of the two-dimensional transonic full potential equation. In Ref. 2, it was found that because of the type dependent, or mixed elliptic/hyperbolic nature of the crossflow, transonic techniques such as those developed by Jameson[3] could be used to determine numerical solutions. The conical flow problem was extended to include three-dimensional flow by Grossman and Siclari[4] using a fully implicit marching technique where each marching step requires an implicit crossflow solution. These schemes have all used Successive-Line-Over-Relaxation (SLOR) as their basis for numerical solution of the nonconservative full potential equation. For the nonconical problem, it was found by Siclari[5] that accuracy could be enhanced by isentropically fitting the bow shock and numerical efficiency optimized by a judicious selection of the sweep direction.

As the procedure for solving the full potential equation for supersonic problems matured, other investigators have established similar methods. Shankar et al[6,7], using a semi-implicit marching technique with a density linearization of the conservative full potential equation, has also shown success. Comparisons of Shankar's conservative approach with the present nonconservative formulation in Ref. 6 show remarkably excellent agreement considering the conservative versus nonconservative treatments. The semi-

implicit formulation of Ref. 6 or 7 requires some CFL constraints, unlike the present fully implicit formulation which has no CFL constraints. Sritharan[8] and Bradley et. al[9] have also developed conservative formulations for solving the conical problem. Comparisons with the present approach that are shown in Reference 8 exhibit excellent agreement except for the typical conservative/nonconservative disparities that occur in the vicinity of the captured crossflow shock.

In the present work, two basic topics are studied with the aim of broadening the applicability and usefulness of the present method encompassed within the computer code NCOREL (NONConical RELaxation, see Ref. 18) for the treatment of supersonic flow problems. The first topic is that of computing efficiency. Accelerated schemes exist and are in current use for transonic flow problems. One such scheme is the approximate factorization (AF) method. This study will develop and apply an AF scheme to the supersonic flow problem. The second topic that will be addressed will be the computation of wake flows. The proper modeling of wake flows is important for multi-component configurations such as wing-body and multiple lifting surfaces where the wake of one lifting surface will have a pronounced effect on a downstream body or other lifting surface. This is an interim report of a larger study. A final report will cover these topics and other topics presently under investigation.

## 2. APPROXIMATE FACTORIZATION SCHEMES

Numerical techniques are investigated that show promise for accelerating convergence in comparison with the standard SLOR methods. The primary candidate for this is the alternating-direction-implicit (ADI)[10] or, as it is more commonly referred to in its application to nonlinear transonic flows, approximate factorization (AF) schemes. These AF schemes have been applied successfully to a variety of transonic flow problems. Initially, AF schemes were applied to the Transonic Small Disturbance (TSD) equation by Ballhaus, et al[11]. Holst[12] successfully applied an AF2 type scheme to the conservative full potential equation for transonic flows. The nonconservative full potential equation was treated successfully by Baker[13,14] for 2D transonic flows and should be applicable to the nonconservative full potential supersonic/transonic crossflow problem of the present study. Two basic AF algorithms are considered, ADI or AF1 and the AF2 scheme which splits one of the second derivatives into two first-order derivative operators. The latter scheme has reportedly been the most stable in supersonic flow regions for the transonic flow problem.

### 2.1 BASIC FORMULATION

The nonconservative form of the 3D full potential equation is written in a spherical coordinate system ($\omega$, $\psi$, r). The governing equation is then transformed via a conformal stereographic projection to (p, q, t) coordinates and further by a crossflow conformal Jowkowski mapping to ($\rho$, $\theta$, R) coordinates. In terms of a reduced potential F, where $Q = \nabla\phi + q_\infty$ and $\phi = RF(\rho,\theta,R)$, the full potential equation can be written as

$$\frac{(a^2-U^2)}{\rho^2} F_{\theta\theta} - \frac{2UV}{\rho} F_{\rho\theta} + (a^2-V^2)F_{\rho\rho} + \ldots$$

$$= RH\ [(W^2-a^2)RHh_1 + 2WV][h_1F_{\rho\rho} + \frac{h_2}{\rho} F_{\rho\theta} + F_{\rho R}$$

$$+ \frac{1}{\rho}\ [(W^2-a^2)RHh_2 + 2WU][h_1F_{\rho\theta} + \frac{h_2}{\rho} F_{\theta\theta} + F_{\theta R}]$$

$$+ RH(W^2-a^2)[h_1F_{\rho R} + \frac{h_2}{\rho} F_{\theta R} + F_{RR}] + \ldots \qquad (1)$$

where U, V, and W are the velocities in the $\theta$, $\rho$, and R directions, respectively, and H is the combined metric of the two mappings. In general, the conformal mapping in the crossflow plane leads to nonorthogonal coordinate derivatives if the mapping singularity is a function of r. This mapping dependence on r leads to mesh derivatives defined as $h_1 = \rho_r$ and $h_2 = \rho\theta_r$. The radial marching direction r, remains unchanged due to the transformations, or $r = t = R$. The details of the mappings and coefficients can be found in Ref. 2 and 4.

Unlike transonic flow, the supersonic flow problem is contained within a finite crossflow mesh bounded by a bow shock. The bow shock may be captured within a prescribed outer boundary[2,4] or the bow shock can be fitted as the outer boundary[5] using the isentropic shock jump conditions.

A shearing transformation is applied to Eq (1), between the body $\rho = B(\theta, R)$ and outer boundary or bow shock $\rho = C(\theta, R)$, where

$$\begin{aligned} X &= \theta \\ Y &= \frac{\rho - B}{C - B} \\ Z &= R \end{aligned} \tag{2}$$

which yields a final rectangular computational mesh.

Equation (1) can be represented as the sum of a conical plus a nonconical operator, in the form

$$L(\phi_{i,j}) = L_C(\phi_{i,j}) + R \cdot L_{NC}(\phi_{i,j}) \; . \tag{3}$$

The nonconical coefficients on the RHS of Eq (1) all have an R dependence and vanish identically at R = 0 for the quasi-two-dimensional conical flow problem.

## 2.2 CONICAL FLOWS

For conical flows, after applying the shearing transformation, Eq (1) can be written as

$$L_C(\phi_{i,j}) = A_1 F_{XX} + A_2 F_{XY} + A_3 F_{YY} + \cdots \tag{4}$$

where

$$A_1 = \frac{(a^2-U^2)}{\rho^2}$$

$$A_2 = \frac{-2UV}{\rho} Y_\rho + 2\frac{(a^2-U^2)}{\rho^2} Y_\theta \qquad (5)$$

$$A_3 = (a^2-V^2)Y_R^2 - \frac{2UV}{\rho} Y_\rho Y_\theta + \frac{(a^2-U^2)}{\rho^2} Y_\theta^2 .$$

Equation (4) closely resembles the nonconservative form of the 2-D transonic flow equation. The difference is that the type dependency of the conical part of Eq (1) or Eq (4) is linked to the nature of the crossflow velocity defined by $Q_c^2 = U^2 + V^2$. An upwind bias in the difference equations must occur when the crossflow velocity is supersonic or $Q_c^2 > a^2$. The crossflow velocity component V is always negative and toward the body surface. The U component of velocity can be positive or negative depending upon the geometry and angle of attack. Equation (4) has heretofore been solved successfully using transonic SLOR techniques[2,4] and the rotated difference scheme of Jameson[3].

The principal part of Eq (4) can be rewritten in a rotated difference format as, for $Q_c^2 > a^2$

$$A_1 F_{XX} + A_2 F_{XY} + A_3 F_{YY} = (a^2-Q_c^2) F_{ss} + a^2 F_{nn} \qquad (6)$$

where

$$F_{ss} = \frac{V_1^2}{Q_c^2} F_{YY} + \frac{2U_1V_1}{Q_c^2} F_{XY} + \frac{U_1^2}{Q_c^2} F_{XX}$$

$$F_{nn} = \frac{U_2^2}{Q_c^2} F_{YY} - \frac{2U_2V_2}{Q_c^2} F_{XY} + \frac{V_2^2}{Q_c^2} F_{XX}$$

and

$$U_1 = U/\rho \quad , \quad V_1 = VY_\rho + \frac{UY_\theta}{\rho}$$

$$V_2 = V/\rho \quad , \quad U_2 = UY_\rho - \frac{VY_\theta}{\rho} \, .$$

An upwind bias is applied to the finite difference representation of the $F_{ss}$ terms, and central differences are used for the $F_{nn}$ terms in supersonic crossflow regions.

The following sections will present an adaptation of the two basic AF algorithms, ADI or AF1 and AF2, to the present supersonic flow problem.

2.2.1 AF1 Factorization

An ADI or AF1 type factorization can be applied to the principal terms of Eq (4), for subsonic crossflow $Q_c^2 < a^2$, in the form

$$\left(\alpha - A_1 \frac{\overset{+}{\delta}_X \overset{-}{\delta}_X}{\Delta X^2}\right)\left(\alpha - A_3 \frac{\overset{+}{\delta}_Y \overset{-}{\delta}_Y}{\Delta Y^2}\right) \Delta_{i,j}^{n+1} = \alpha\omega L_c(\phi_{i,j}^{n}) \qquad (7)$$

where $\Delta_{i,j}$ is the correction to the reduced potential $F_{i,j}$ or $\Delta_{i,j} = F_{i,j}^{n+1} - F_{i,j}^{n}$. $\omega$ is a relaxation parameter and $L_c(\phi_{i,j})$ is the residual of Eq (4) at the nth iteration. $\alpha$ is an acceleration parameter which is varied in a cyclic fashion during the iteration process. The two first-order difference operators result in a second-order central difference. The first-order operators are defined as

$$\begin{aligned} \overset{+}{\delta}_X &= (\ )_{i+1,j} - (\ )_{i,j} \\ \overset{-}{\delta}_X &= (\ )_{i-1,j} - (\ )_{i,j} \\ \overset{+}{\delta}_Y &= (\ )_{i,j+1} - (\ )_{i,j} \\ \overset{-}{\delta}_Y &= (\ )_{i,j} - (\ )_{i,j-1} \end{aligned} \qquad (8)$$

The basic premise behind an approximate factorization scheme can be revealed if the LHS of Eq (7) is expanded and terms not resembling those of Eq (4) are neglected, or

$$\left(A_1 \frac{\overset{+}{\delta}_X \overset{-}{\delta}_X}{\Delta X^2} + A_3 \frac{\overset{+}{\delta}_Y \overset{-}{\delta}_Y}{\Delta Y^2}\right)\Delta_{i,j}^{n+1} = -\omega L_c(\phi_{i,j}^n) \quad . \tag{9}$$

If $\omega = 1$, Eq (9) would be equivalent to solving Eq (4) with the cross derivative evaluated using old values of the potential. Equation (9) is typically solved in a two-step format by defining an intermediate variable, $G_{i,j}$, where

$$\left(\alpha - A_1 \frac{\overset{+}{\delta}_X \overset{-}{\delta}_X}{\Delta X^2}\right) G_{i,j}^{n+1} = \alpha\omega L_c(\phi_{i,j}^n)$$

$$\left(\alpha - A_3 \frac{\overset{+}{\delta}_Y \overset{-}{\delta}_Y}{\Delta Y^2}\right) \Delta_{i,j}^{n+1} = G_{i,j}^{n+1} \quad . \tag{10}$$

Equation (10) represents two tridiagonal systems of equations involving differences only in the computational X or Y direction. Equation (10) must be modified in regions of supersonic crossflow to include the proper upwind bias. The following form of the supersonic crossflow factorization is essentially identical to the AF1 scheme of Baker[13,14] equation. Hence, for $Q_c^2 > a^2$ ,

$$\left(\alpha - A_{1c} \frac{\overset{+}{\delta}_X \overset{-}{\delta}_X}{\Delta X^2} - K_1 A_{1u} \frac{\overset{+}{\delta}_X \overset{-}{\delta}_X}{\Delta X^2} - K_2 A_{1u} \frac{\overset{+}{\delta}_X \overset{-}{\delta}_X}{\Delta X^2}\right) G_{i,j}^{n+1} = \alpha\omega L(\phi_{i,j}^n) \tag{11}$$

$$\left(\alpha - A_{3c} \frac{\overset{+}{\delta}_Y \overset{-}{\delta}_Y}{\Delta Y^2} - A_{3u} \frac{\overset{+}{\delta}_Y \overset{-}{\delta}_Y}{\Delta Y^2}\right) \Delta_{i,j}^{n+1} = G_{i,j}^{n+1} \quad .$$

The central (subscript c) and upwind coefficients (subscript u) are given by the rotated difference scheme Eq (6) as

$$A_{1c} = \frac{V_2^2}{Q_c^2} \quad , \quad A_{3c} = \frac{U_2^2}{Q_c^2}$$

$$A_{1u} = \frac{(a^2 - Q_c^2)}{Q_c^2} U_1^2 \quad , \quad A_{3u} = \frac{(a^2 - Q_c^2)}{Q_c^2} V_1^2 \, . \tag{12}$$

The first factor allows for the U component of velocity to be positive or negative, where if

$$U > 0, \quad K_1 = 1, \quad K_2 = 0$$

$$U < 0, \quad K_1 = 0, \quad K_2 = 1. \tag{12a}$$

As mentioned earlier, the V velocity is always negative for supersonic crossflow and, hence, only forward upwind differences occur in the second factor.

In general, the first factor involves a pentadiagonal matrix and the second factor a quadradiagonal matrix. As suggested by Baker[13], these differences can be replaced by

$$\overset{+}{\delta}_X \overset{+}{\delta}_Y = (\;)^{n+1}_{i,j} - (\;)^{n+1}_{i,j} - (\;)^{n}_{i-1,j} + (\;)^{n}_{i-2,j}$$

$$\overset{+}{\delta}_X \overset{+}{\delta}_X = (\;)^{n+1}_{i,j} - (\;)^{n+1}_{i+1,j} - (\;)^{n}_{i+1,j} + (\;)^{n}_{i+2,j} \tag{13}$$

$$\overset{+}{\delta}_Y \overset{+}{\delta}_Y = (\;)^{n+1}_{i,j} - (\;)^{n+1}_{i,j+1} - (\;)^{n}_{i,j+1} + (\;)^{n}_{i,j+2} \, .$$

This reduces the set of Eq (11) to the following tridiagonal form, for $Q_c^2 > a^2$ ,

$$\left(\alpha - A_{1c} \frac{\overset{+}{\delta}_X \overset{+}{\delta}_X}{\Delta X^2} - I_s \frac{A_{1u}}{\Delta X^2} (K_1 \overset{+}{\delta}_X + K_2 \overset{+}{\delta}_X)\right) G^{n+1}_{i,j} = \alpha\omega L_c(\phi^n_{i,j}) \tag{14}$$

$$\left(\alpha - A_{3c} \frac{\overset{+}{\delta}_Y \overset{+}{\delta}_Y}{\Delta Y^2} + A_{3u} \frac{\overset{+}{\delta}_Y}{\Delta Y^2}\right) \Delta^{n+1}_{i,j} = G^{n+1}_{i,j}$$

where, for $U > 0$, $I_s = 1$ and $U < 0$, $I_s = -1$.

### 2.2.2 AF2 Factorization

The AF2 algorithm has been found by several investigators[11,12] to generally be the more stable AF factorization for transonic flows. In the AF2 factorization, one of the second derivatives is split between the two factors. Following a similar AF2 factorization used by Baker[13], for subsonic crossflow, $Q_c^2 < a^2$, the AF2 algorithm becomes

$$\left(\frac{-\alpha}{H_m}\frac{\overleftarrow{\delta}_Y}{\Delta Y} - A_1\frac{\overleftarrow{\delta}_X\overleftarrow{\delta}_X}{\Delta X^2} \quad \alpha + A_3 H_m\frac{\overleftarrow{\delta}_Y}{\Delta Y}\right)\Delta_{i,j}^{n+1} = \alpha\omega L_c(\phi_{i,j}^n) \ . \tag{15}$$

This form of factorization is thought to be more stable since the Y operator in the first factor yields a $\phi_{Yt}$ term, unlike the $\phi_t$ term of the AF1 scheme[14]. The term $H_m$ in the two factors accounts for the transformation derivatives of the mapped and sheared mesh. As illustrated by Catherall[15], the proper splitting of these transformation derivatives can yield optimum convergence, and neglecting these derivatives can considerably degrade convergence. The coefficient $A_3$ in Eq (4) contains the shearing transformation derivatives $Y_\rho$ and $Y_\theta/\rho$. The mapped plane $(\rho,\theta)$ velocities, V and U respectively, contain the metric $H(\rho,\theta)$ of the two mappings. Hence, a suitable form for the factor $H_m$ might be

$$H_m = \frac{\Delta Y}{\Delta X}\frac{Y_\rho}{H} \quad \text{or} \quad \frac{\Delta Y}{\Delta X}\frac{1}{H}\left(Y_\rho - \frac{Y_\theta}{\rho}\right) \ . \tag{16}$$

The first-order forward difference operator on Y is placed in the first factor since this term does not switch for supersonic crossflow conditions. For supersonic crossflow, the AF2 factorization is modified to include an upwind bias and a tridiagonal form as

$$\left(\frac{-\alpha}{H_m}\frac{\overleftarrow{\delta}_Y}{\Delta Y} - A_{1c}\frac{\overleftarrow{\delta}_X\overleftarrow{\delta}_X}{\Delta X^2} - \frac{I_s A_{1u}}{\Delta X^2}(K_1\delta_X + K_{2d}\delta_X)\right)G_{i,j}^{n+1} = \alpha\omega L_c(\phi_{i,j}^n) \tag{17}$$

$$\left(\alpha + A_{3c}H_m\frac{\overleftarrow{\delta}_Y}{\Delta Y} + A_{3u}H_m\frac{\overleftarrow{\delta}_Y}{\Delta Y}\right)\Delta_{i,j}^{n+1} = G_{i,j}^{n+1} \ .$$

Since the forward Y operator is included in the first factor, the sweep is constrained to be toward the body surface or decreasing J.

An alternate factorization to the AF2 scheme described above would be to split the X-derivative. Unlike transonic flow, the difficulty in splitting the X-derivative in the supersonic problem is that the U velocity in the supersonic crossflow region can be either positive or negative. This occurs primarily at the captured bow shock. In transonic flow, the X or U velocity direction is much like the Y direction of the present problem in that a negative supersonic U velocity is unlikely to occur. Hence, there is no first order X operator that, in general, does not switch. One could propose a scheme where the factorization is set up for $U < 0$, and if $U > 0$, the upwind coefficient is either neglected or a shift operator is imposed. This scheme was found to be unstable or would not work for this problem.

Other AF2 factorizations were considered, including the AF3 factorization of Baker[13] where both coefficients are brought into the first factor. This would seem to be a candidate for a faster scheme since the differential operators would not act on the coefficients and lead to spurious terms. Baker[13], in fact, has reported his AF3 scheme to be considerably faster than either the AF1 or AF2 schemes. Unfortunately, this scheme could not be applied successfully to Eq (17).

### 2.2.3 Boundary Conditions

Figure 1 illustrates the conformally mapped and sheared computational crossflow plane domains. Symmetry conditions are imposed at $\theta = \pm \pi/2$ or I = 2 and IC for the symmetric half plane problem. Hence, periodic end conditions apply on Y = constant lines. On X = constant lines, J = 2 corresponds to the body surface and J = JMAX corresponds either to the outer boundary (BSC) or the bow shock (BSF). In both the bow shock capture or fit methods, the outer boundary has the same condition that the correction to the potential vanish, or

$$\Delta_{i,jmax} = 0 \quad . \tag{18}$$

A dummy row or Y = constant line at J = 1 is used to implement the body boundary condition of flow tangency. This condition relates the values of the correction at J = 1 to those at J = 3, or for conical flow yields:

$$\Delta_{i,1} = \Delta_{i,3} \cdot \tag{19}$$

In this way, central derivatives can be used for $F_Y$ and the body surface coordinate line can be treated like any other coordinate line.

The order of the factors in both AF schemes were chosen so that the first sweep is carried out on Y = constant lines. This was chosen over the reverse factorization so that periodic end conditions could be imposed on the intermediate variable G, or

$$\begin{aligned} G_{1,j} &= G_{3,j} \\ G_{IC+1,j} &= G_{IC-1,j} \end{aligned} \tag{20}$$

which most certainly is a reasonable assumption. If the factors in the AF schemes are reversed, then somewhat arbitrary boundary conditions must be imposed on the intermediate variable G. The end conditions (18) and (19) then apply to the second sweep on the X = constant lines.

### 2.2.4 Temporal Damping

It has been indicated that the basic AF1 scheme may be unstable in supersonic regions. To allow for this possibility, the AF1 scheme has been generalized to include an explicit temporal damping $F_{st}$ (e.g., $\phi_{st}$) term. Jameson's generalized AF scheme[16] includes similar terms in both factors. In Reference 12, it was indicated that this term may also be required in the AF2 scheme. It was found that adding this term explicitly to the first factor was sufficient to maintain stability for flows with captured shocks. This stability or temporal damping term has the form[5]:

$$-\varepsilon\, \delta_{st} = -\varepsilon \frac{V_1}{Q_c} \overleftrightarrow{\delta}_Y + \frac{U_1}{Q_c} \left(K_1 \overleftrightarrow{\delta}_X + K_2 \overleftrightarrow{\delta}_X\right)$$

where

$$\frac{K}{|1-M_c|} < \varepsilon < \varepsilon_{max} K \tag{21}$$

$$\varepsilon_{max} = 10$$

In general, the addition of the temporal damping slows convergence. Hence, the form of the factor $\varepsilon$ was chosen to maximize the damping in the vicinity of sonic lines or across shocks so as not to cause an overall degradation in the convergence rate. The constant K is chosen to be as small as possible for the optimum convergence.

In general, there are no restrictions on the sweep due to the velocity directions in an AF1 scheme. The first sweep can be from the outer boundary to the body surface or the reverse. In order to properly include temporal damping in the AF1 scheme, the first sweep must be in the direction of the supersonic crossflow. This requires that the Y = constant sweep must be towards the body or decreasing J since $V < 0$.

In the supersonic problem (unlike the transonic case), it was observed that the AF1 scheme required little or no temporal damping except for the most difficult cases whereas the AF2 scheme required considerably higher values of $\varepsilon$ for the strong Y-shock solutions.

### 2.2.5 Acceleration Parameter

For the AF1 scheme, the maximum and minimum values of the acceleration parameter $\alpha$ were taken as

$$\alpha_{max} = A_{max} \quad \frac{1}{\Delta X^2}, \frac{1}{\Delta Y^2}$$

$$\alpha_{min} = A_{min} \quad \frac{1}{\Delta X}, \frac{1}{\Delta Y} . \tag{22}$$

The coefficients $A_{min}$ and $A_{max}$ were taken anywhere from 0.5 to 4.0 for all the cases computed. The convergence rate could be affected by as much as a factor of two by a judicious choice of these parameters.

In the AF2 scheme, these parameters were chosen as

$$\alpha_{max} = A_{max} \quad \frac{1}{\Delta X}, \frac{1}{\Delta Y}$$

$$\alpha_{min} = A_{min} \quad \frac{1}{\Delta X}, \frac{1}{\Delta Y} \tag{23}$$

where $A_{min}$ varied between 0.5 and 6 and $A_{max}$ between 3 and 6. Typically, unity for $A_{min}$ and three for $A_{max}$ was sufficient for most cases. The theoretical value of $\alpha_{min} = 1$ or 2 could never be achieved, possibly due to the effect of the various coordinate transformations.

For both AF schemes, the cyclic variation of $\alpha$ took the form

$$\alpha_I = \alpha_{max} \left( \frac{\alpha_{min}}{\alpha_{max}} \right)^{\frac{I-1}{IMAX-1}} \quad \text{for } I = 1, \text{ IMAX} \tag{24}$$

where IMAX = 3 for the AF1 scheme and IMAX = 6 for the AF2 scheme. The minimum number of cycles seemed to be the best choice for the AF1 scheme. The convergence rate of the AF2 scheme was affected insignificantly for IMAX between 3 and 6. Further increase in IMAX reduced the convergence rate. In all of the cases computed, $\omega_{AF1} = 1.50$ or 1.70 and $\omega_{AF2} = 1.33$. Departures from Eq (24) did not seem to affect significantly the convergence rates.

### 2.2.6 Conical Results

Two techniques are available for the computation of supersonic conical flows: the bow shock capture[2,4] (BSC) and bow shock fit[5] (BSF) methods. In the BSC method, an outer mesh boundary $\rho = C(\theta)$ is prescribed, and the bow shock is captured within this boundary. The BSC method is a more stringent test of the AF schemes in that two shocks may be present in the flow, the bow shock (Y-shock) and an embedded crossflow shock (X-shock) as illustrated in Fig. 1. The bow shock is the most critical in that its position and strength largely determine the internal flow. The bow shock also extends around the entire field encompassing more points than the embedded crossflow shock. The BSF method fits the bow shock as the outer boundary and, hence, eliminates the bow shock from the internal flow calculation; if an embedded supersonic crossflow region is not present, the internal flow problem becomes elliptic. The conical convergence rate of the BSF method is largely determined by the implicit shock fitting procedure where the shape of the boundary is updated and usually underrelaxed until the isentropic shock jump condition is fulfilled at each shock mesh point. The conical BSF method also requires more

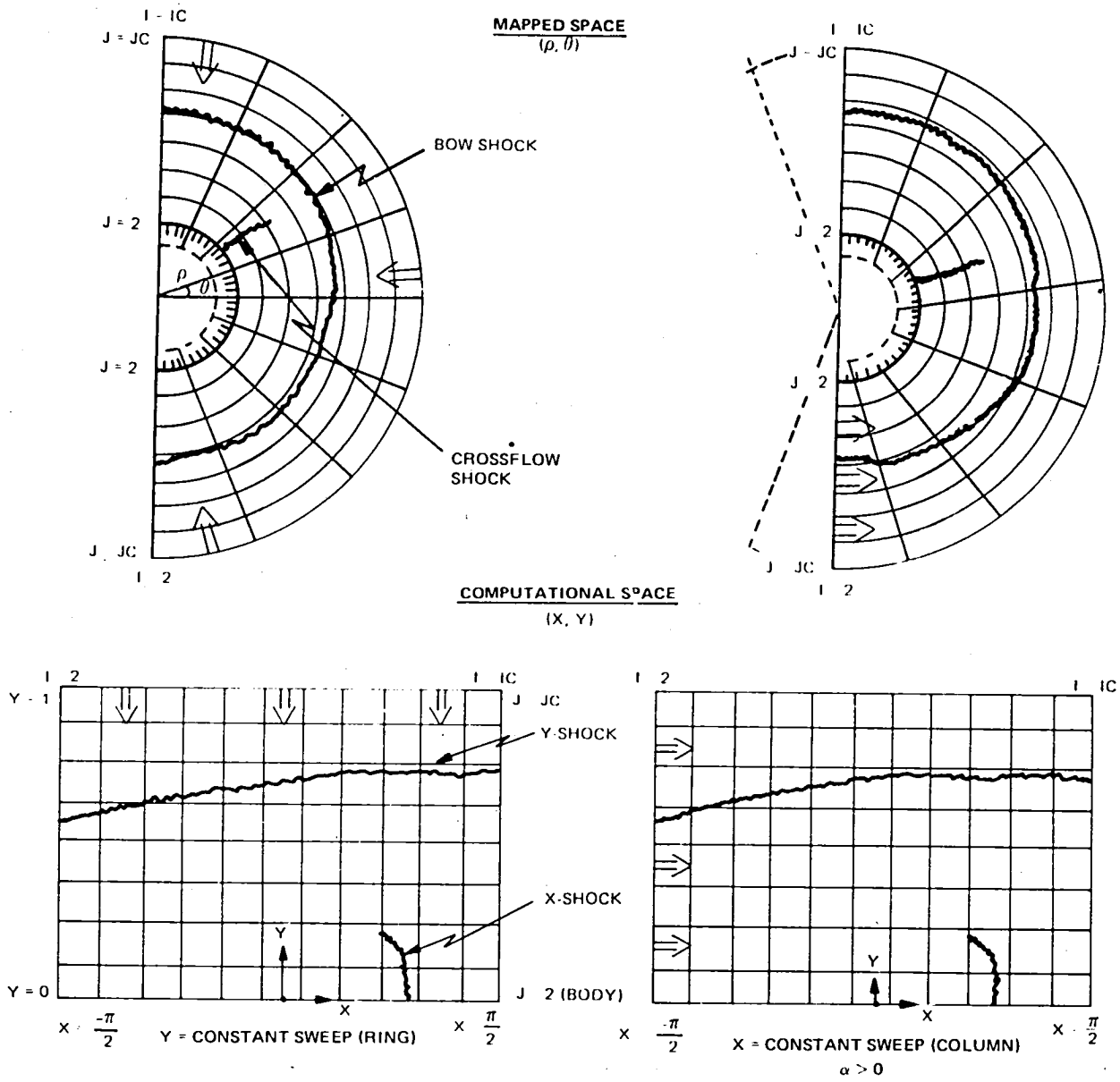


1264-001(T)

**Fig. 1 Sweep and Mesh Definitions**

computational time per iteration because the crossflow mesh and metrics must be recomputed for each iteration after the bow shock shape has been updated.

For conical flow, the BSC method is used primarily to evaluate the AF schemes. Figure 2 shows the effect of reversing the order of the factors in the AF1 scheme for a thin elliptic cone at $M_\infty = 2.0$, $\alpha = 0°$. The AF1XY scheme represents the order of the factors indicated in Eq (7) and (14) where periodic end conditions are used for the intermediate variable G. The factors were then reversed (AF1YX) with the first sweep occurring on X = constant lines. Two different boundary conditions were used: setting $G_{i,1} = 0$ as the end condition in the tridiagonal on the dummy row below the body; and using $G_{i,1} = G_{i,3}$ as the periodic end condition, as is the case for the condition on the correction $\Delta_{i,1}$.

All three cases were run with the same $\alpha$ variation. As shown in Fig. 2, the results are quite sensitive to the boundary condition on the intermediate variable, and making the intermediate variable mimic the correction seems to be the best choice. Even with this boundary condition, the YX factorization does not give identical results to the XY factorization and seemed to be somewhat more sensitive to the $\alpha$ variation. Hence, the AF1XY scheme was used for all the computations.

Figure 3 shows a comparison of the convergence rate of the maximum residual for the AF1 and SLOR schemes for a thin subsonic leading edge elliptic cone ($\theta_c = 20°$, $\delta_c = 2°$) on a (48 x 38) crossflow mesh at $M_\infty = 2$ and angles of attack $\alpha = 0°$ and $10°$. The SLOR scheme found to be optimum for this problem in Ref. 5 is one that sweeps around the body on X = constant lines. The "column" SLOR scheme was found to be two to five times faster than the alternate SLOR scheme which sweeps toward the body on Y = constant lines. It is interesting to note that after one or two orders of magnitude reduction in the maximum residual, the SLOR scheme for the supersonic freestream problem does not exhibit the typical slowdown in convergence rate that occurs in transonic flow problems. A break in the SLOR curve occurs after one order of magnitude but remains linear for further reductions. It is also interesting to note that the SLOR convergence rates of the $\alpha = 0°$ and $\alpha = 10°$ flows are not dramatically different, both taking about 350 to 400 iterations, considering that the 10° case is a multishocked flow. At $\alpha = 10°$, a strong crossflow shock develops but is evidently overshadowed by the convergence of the captured bow shock. The AF1

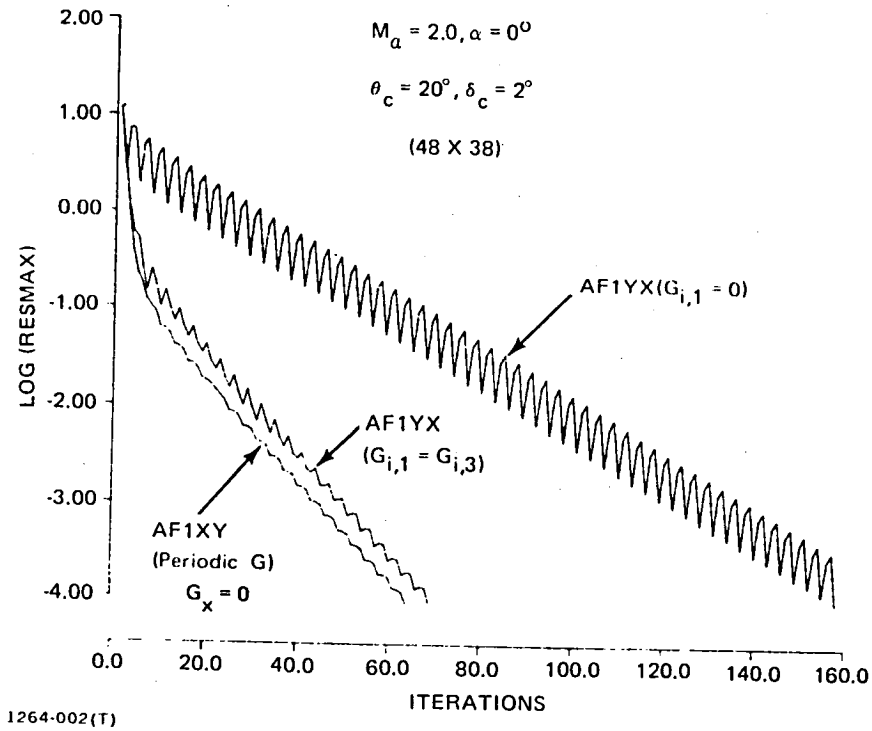


**Fig. 2 Effect of Surface Boundary Condition and Factor Sequence on the AF1 Scheme (BSC) Convergence Rate**

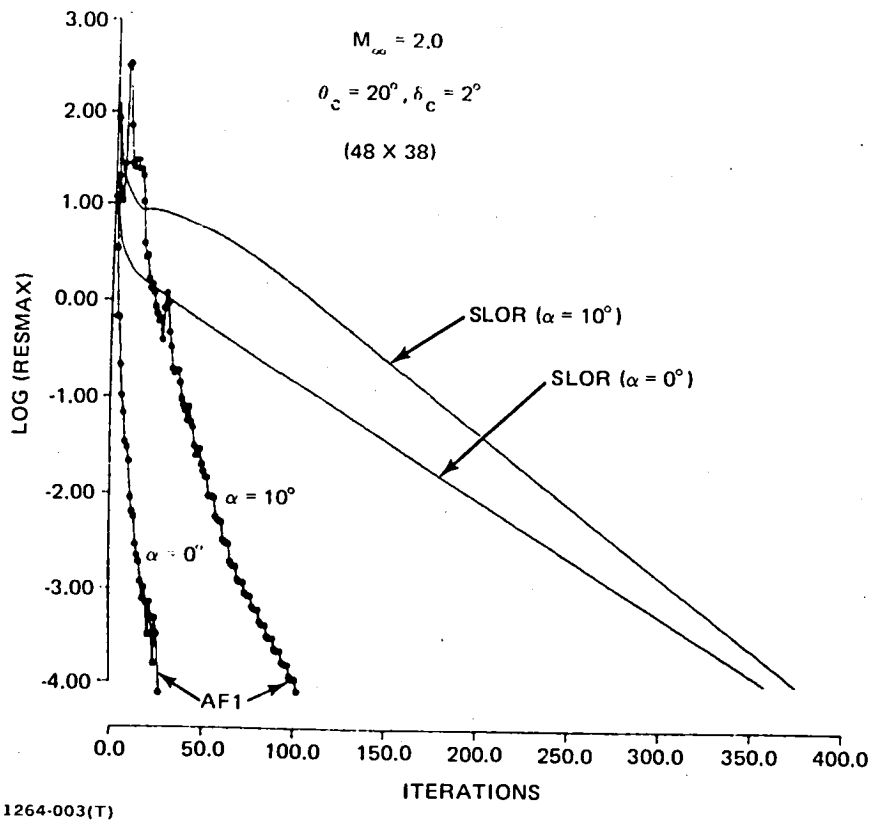


**Fig. 3 Comparison of AF1 Convergence Rate with SLOR (BSC)**

scheme at $\alpha = 0°$ converges very quickly. Essentially, these flows are converged when the maximum residual reaches $10^{-2}$. For $\alpha = 0°$, this occurs at about 10 iterations or when the log (RESMAX) = -2. The AF1 scheme is an order of magnitude faster than the SLOR scheme for $\alpha = 0°$. As the angle of attack increases, the AF1 scheme slows down by a factor of 3 while the SLOR remains about the same. Overall, the AF1 scheme is at least three times faster iteration wise than the SLOR scheme. The relaxation factor was 1.5 for these cases in both schemes, and three cycles were used in the AF1 scheme. A larger number of cycles did not seem to enhance convergence. Figure 4 shows the surface pressure distributions for the elliptic cone computed in Fig. 3 at $\alpha = 0°$, 5°, and 10° and $M_\infty = 2.0$ on a finer mesh. Both $\alpha = 5°$ and $\alpha = 10°$ have crossflow shocks on the leeward surface. Figure 5 shows the computed crossflow streamline pattern at $\alpha = 10°$. As mentioned earlier, the V component of velocity is negative. The crossflow streamlines emanate from the bow shock and travel toward the body surface coalescing at the leeward and windward vortical singualrities. One streamline stagnates on the body and wets the body surface. Also shown is the extent of the embedded supersonic crossflow region, which terminates at the crossflow shock.

Before the AF2 scheme was implemented, the effect of splitting the transformation derivatives between the two factors was studied. Figure 6 indicates the effect of using different forms for the term $H_m$ in Eq (16). If the transformation derivatives are neglected in the factorization, the case could only be run when the $\alpha$ variation was increased significantly. Increasing the minimum value of $\alpha$ generally degrades the convergence rate. The best convergence was achieved when both the metric and the shearing transformation derivatives were included in the term $H_m$. The two curves in Fig. 6 with $H_m$ other than unity were obtained with an alpha variation that diverged when $H_m = 1$. Hence, the AF2 scheme seems to be sensitive to the coordinate transformations, and the convergence rate can be affected significantly. The form of $H_m$ is not considered to be optimum, and further analytical and numerical studies should be conducted to study its effect on the convergence rate. A nonoptimum $H_m$ may also affect the minimum values of $\alpha$ that can be used.

Figure 7 shows a comparison of the convergence rates of the AF1 and AF2 schemes for the elliptic cone of Fig. 3 at $\alpha = 10°$. A comparable convergence

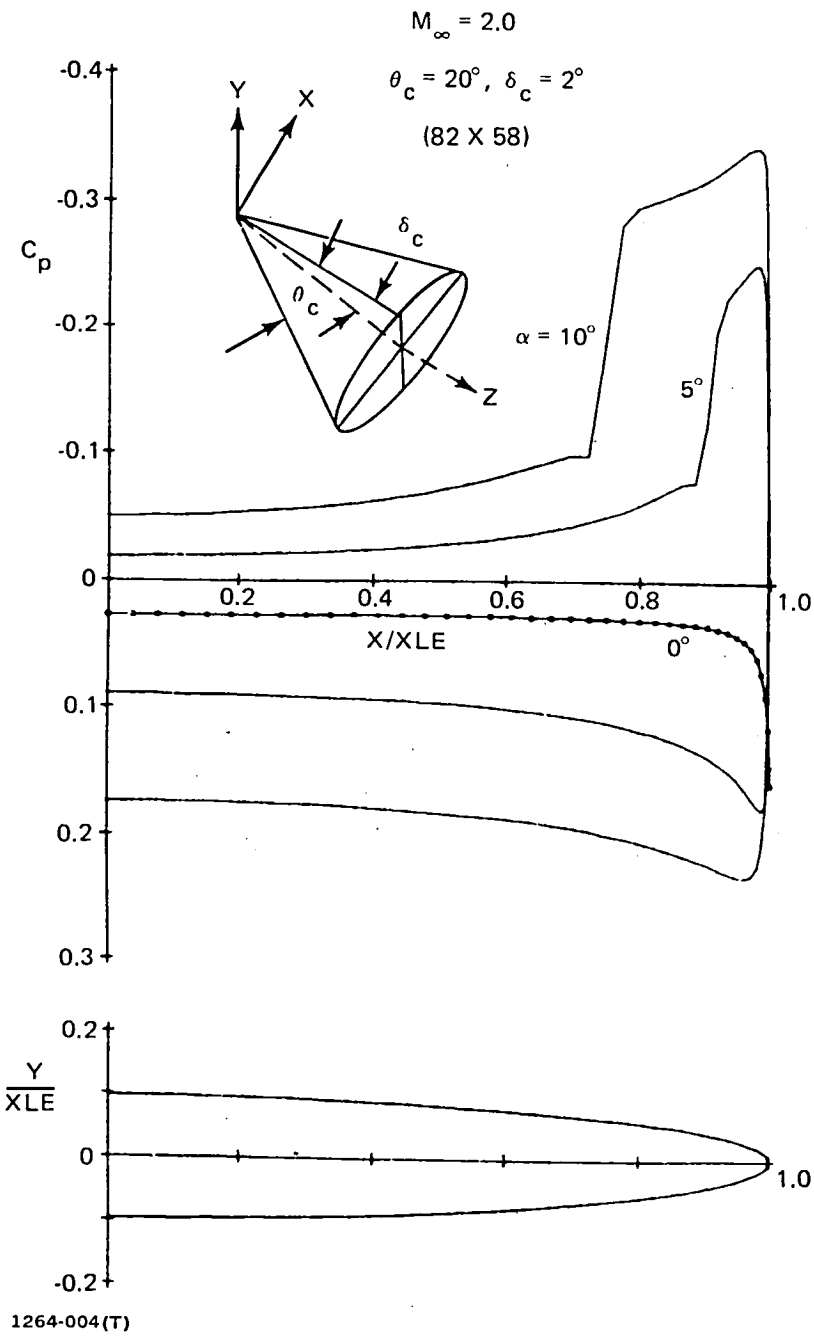


**Fig. 4 Surface Pressure Distributions for Subsonic Leading Edge Elliptic Cone (BSC)**

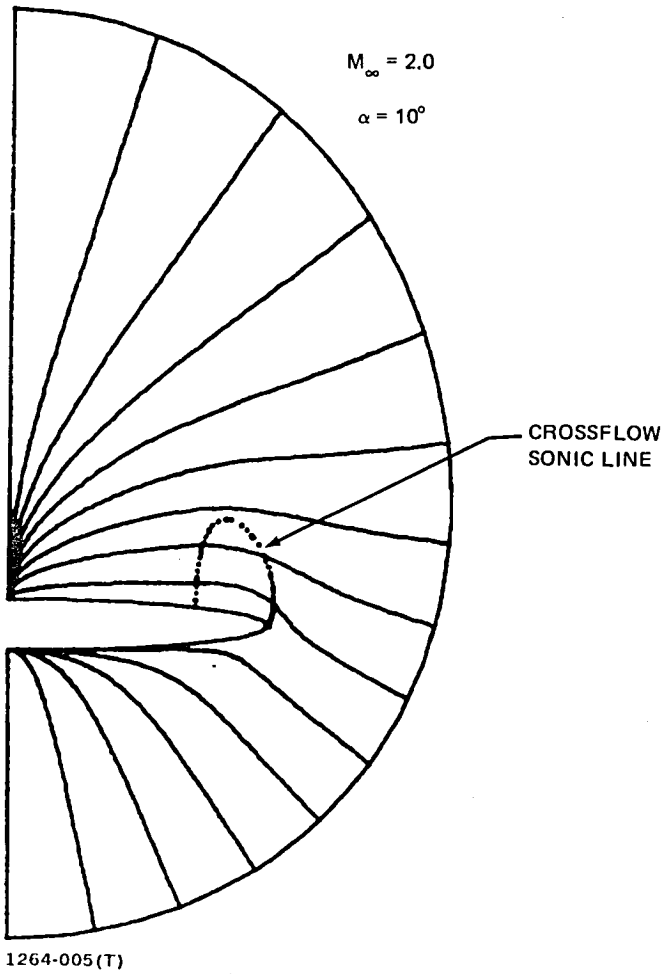


**Fig. 5 Crossflow Streamline Pattern for Subsonic Elliptic Cone (BSF)**

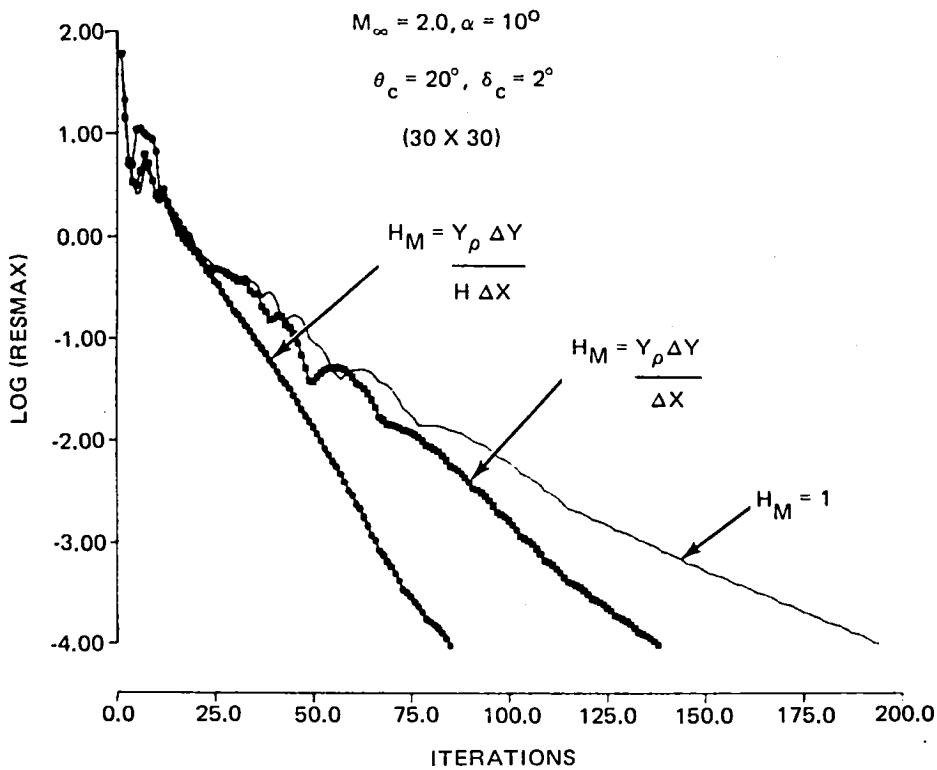


**Fig. 6 The Effect of Transformation Derivatives on the AF2 Scheme (BSC)**

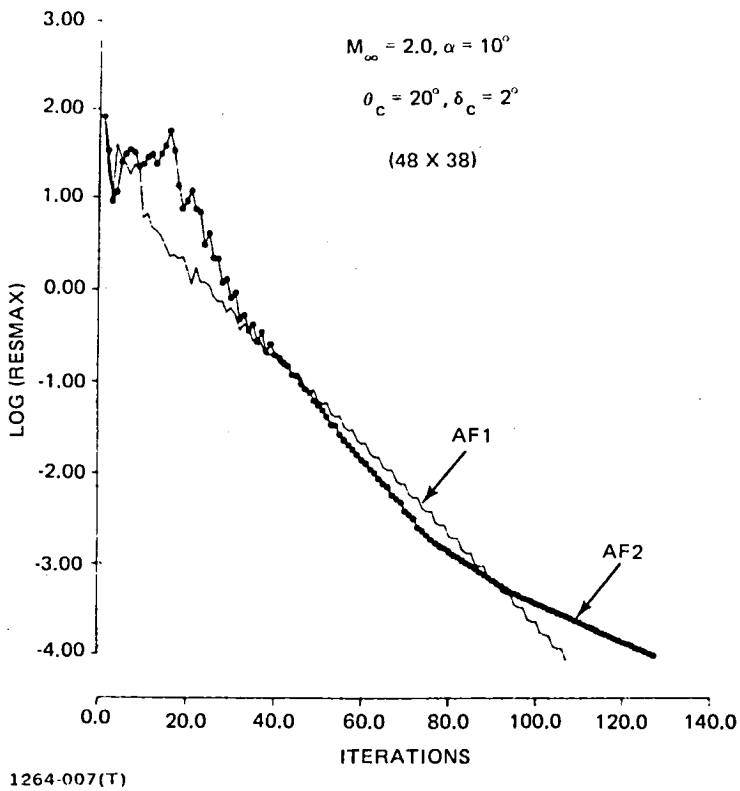


**Fig. 7 Comparison of AF1 and AF2 for a Multi-shock Flow (BSC)**

rate was eventually achieved with the AF2 scheme. Further investigation of the AF2 scheme led to more problems (see Ref. 17) and more sensitivity (i.e., not user friendly) to the choice of acceleration parameters. Hence, the AF2 scheme does not seem to have any advantages over the AF1 scheme and was not further considered for implementation in NCOREL.

### 2.2.7 Mesh Refinement

In Ref. 14, it was observed that for transonic flow, mesh refinement enhanced convergence for SLOR but did not significantly accelerate convergence with the AF schemes. This is apparently not the situation with supersonic flows where the bow shock formation is a critical factor. This is demonstrated in Fig. 8 for the subsonic elliptic cone at $\alpha = 5°$. The mesh refinement in the AF1 scheme yields a factor of three enhancement in convergence rate over the same computation on a single fine mesh. Mesh refinement also enhances the convergence rate of the SLOR scheme. The mesh refined AF1 indicates a factor of six to seven over the mesh refined SLOR result, which is similar to the reduction gained for a single mesh solution.

### 2.2.8 Bow Shock Fit

The AF1 scheme was also adapted to the conical bow shock fit method. In the BSF method, the capture of the bow shock is eliminated from the internal flow field. For any given outer boundary within or coincident with the true bow shock, the internal flow field will quickly converge. Hence, the convergence rate is largely governed by the iteration scheme for determining the bow shock position that satisfies the isentropic shock jump conditions. Typically, the updated bow shock boundary must be underrelaxed at each iteration so as not to disturb the convergence of the internal flow field computation. The bow shock boundary also has to be underrelaxed so as not to overshoot the correct bow shock position, which would cause the internal flow attempt to capture a portion or all of the bow shock, thus leading to divergence. The major advantage in applying the AF schemes to the BSF method is that the correct bow shock information will propagate faster to and around the boundary and allow greater values of the shock relaxation parameter ($\omega_s$), leading to an enhanced overall convergence rate. Figures 9 and 10 illustrate the AF1 convergence rate of the subsonic elliptic cone in comparison to SLOR at $\alpha = 5°$ and 10°, respectively. In Fig. 9 and 10, the maximum residual convergence is shown. In the SLOR curves, the shock relaxation parameter was

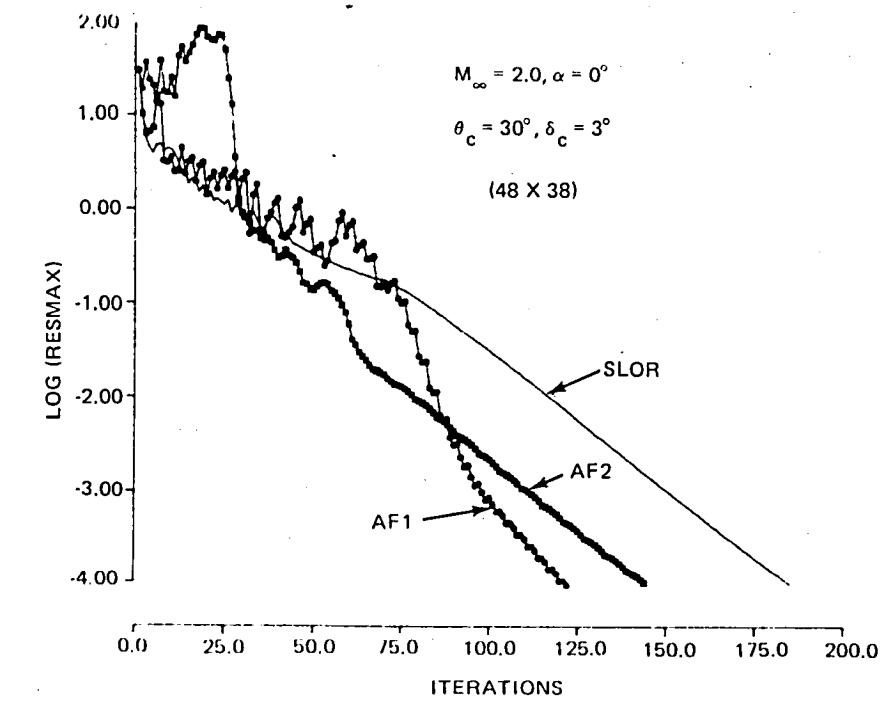


**Fig. 8 Comparison of AF1, AF2 and SLOR Convergence Rates for Elliptic Cone with Sonic Leading Edge (BSC)**

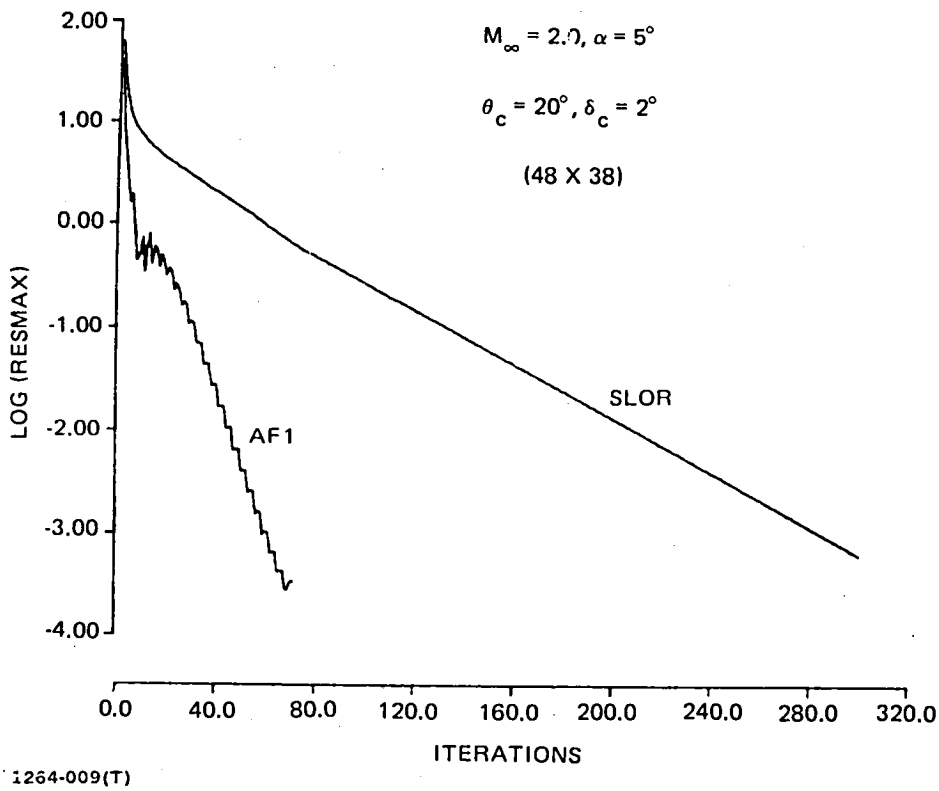


**Fig. 9 Comparison of AF1 and SLOR Convergence Rates for the Bow Shock Fit Method at $M_\infty = 2.0, \alpha = 5°$**

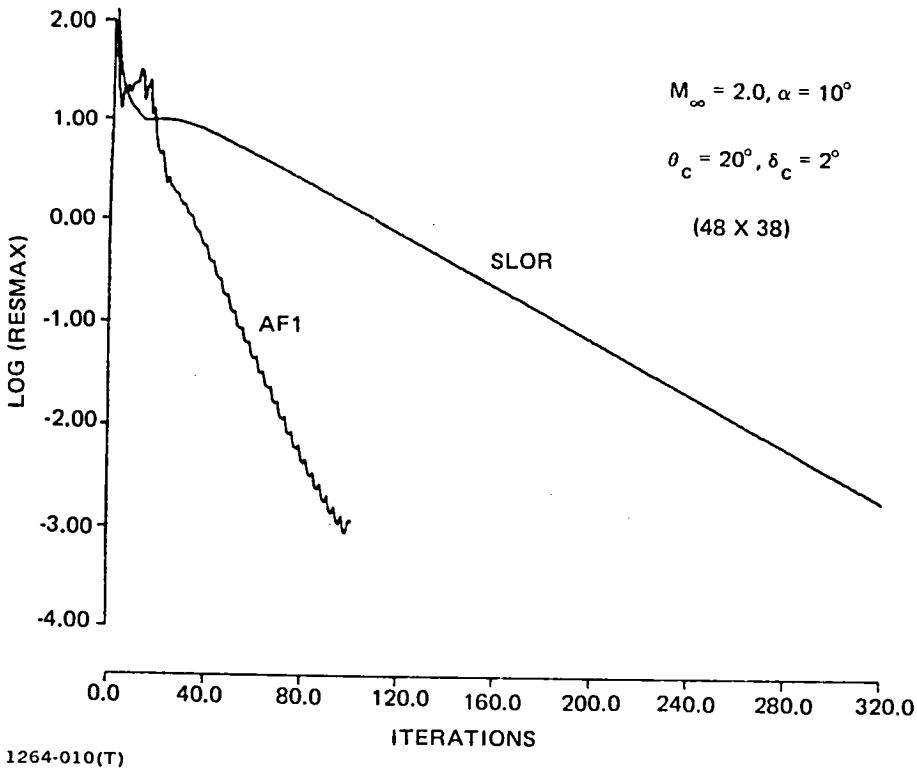


**Fig. 10 Comparison of AF1 and SLOR Convergence Rates for the Bow Shock Fit Method at $M_\infty = 2.0, \alpha = 10°$**

0.75 and 0.50, respectively, for $\alpha = 5°$ and $\alpha = 10°$. Higher values cause divergence of the flow field. It was observed that with the AF1 scheme the shock relaxation parameter did not require under-relaxation for these cases and could be taken to be equal to unity. Hence, in the AF1 scheme both the bow shock and internal flow field converge faster than the SLOR. As a result, a similar enhancement in convergence rate is obtained for the BSF method as compared to the earlier results indicated for the BSC method.

## 2.3 NONCONICAL OR THREE-DIMENSIONAL FLOWS

The AF1 and AF2 schemes both worked well for quasi-two-dimensional conical flow yielding convergence rates two to ten times faster than SLOR. The AF2 scheme was somewhat more sensitive because of the split Y derivative and the need to include the coordinate transformation derivatives in the factorization. Hence, for the present study, the AF1 scheme will be considered for the nonconical or three-dimensional flow problem. When the shearing transformation is applied to Eq (1), the principal terms of the 3-D full potential equation can be rewritten as

$$\begin{aligned} L(\phi_{i,j}) = {} & (A_1 + B_1)F_{XX} + (A_2 + B_2)F_{XY} \\ & + (A_3 + B_3)\,F_{YY} + B_8F_{ZZ} + B_9F_{XZ} \\ & + B_{10}F_{YZ} + B_{11}F_Z + \cdots \end{aligned} \tag{25}$$

where the $B_i$ coefficients represent the additional nonconical R or 3-D terms. The $B_i$ coefficients are rather complicated and are defined in Ref. 4.

The geometry is assumed to be conical at the apex or R = 0 of the configuration. Marching solutions are then obtained on spherical R or Z = constant surfaces. The terms $F_Z$ and $F_{ZZ}$ always have upwind differences, whereas the $F_{XZ}$ and $F_{YZ}$ terms are smoothly switched when mixed subsonic/supersonic crossflow occurs. A first-order accurate $F_{ZZ}$ difference requires information at two previous planes. Initially, the AF1 scheme was applied to the crossflow plane XY terms of Eq (25) with the Z derivatives treated as forcing terms evaluated with old values of the potential. This scheme turned out to be slower and resulted in divergence in many cases when compared to the optimum SLOR, which includes all the principal Z terms in the tridiagonal

matrix. Hence, a factorization was sought that would maintain the XY crossflow convergence rate of the AF scheme and still retain the SLOR efficiency for the Z terms. The following AF1Z factorization was proposed for subsonic crossflow, $Q_c^2 < a^2$:

$$\left(\alpha - (A_1 + B_1)\frac{\overleftarrow{\delta}_X\overrightarrow{\delta}_X}{\Delta X^2} \frac{-B_8}{\Delta Z^2} \frac{-B_9\delta_{Xc}}{2\Delta X\Delta Z} \frac{-B_{11}}{\Delta Z}\right) G_{i,j}^{n+1} = \alpha\omega L(\phi_{i,j}^n) \tag{26}$$

$$\left(\alpha - (A_3 + B_3)\frac{\overleftarrow{\delta}_Y\overrightarrow{\delta}_Y}{\Delta Y^2} - B_{10}\frac{\delta_{Yc}}{2\Delta Y\Delta Z}\right) \Delta_{i,j}^{n+1} = G_{i,j}^{n+1}$$

where $\delta_{Xc}$ and $\delta_{Yc}$ represent second-order, central, first-derivative operators, or

$$\delta_{Xc} = (\ )_{i+1,j} - (\ )_{i-1,j}$$

$$\delta_{Yc} = (\ )_{i,j+1} - (\ )_{i,j-1} \cdot \tag{27}$$

The Z terms (e.g., $F_{ZZ}$) do not factor because of the hyperbolic nature of the problem and hence are added explicity to the two factors.

The $F_{ZZ}$ difference contains the unknown value of the potential at the current station and the two known values of the potential at the two previous stations. Except for the nonconical coefficients of the $F_{XX}$ and $F_{YY}$ terms, the Z terms are added explicitly to each factor. Including the Z terms in the factorization was also necessary to maintain diagonal dominance and convergence. In many cases, neglecting the Z terms in the AF scheme not only slowed convergence but actually resulted in divergence. For supersonic crossflow, the factorization was modified to include the upwind Z terms or, for $Q_c^2 > a^2$,

$$\left(\alpha - A_{1c}\frac{\overleftarrow{\delta}_X\overrightarrow{\delta}_X}{\Delta X^2} - I_s\frac{(A_{1u}+B_1)}{\Delta X^2}(K_1\overleftarrow{\delta}_X - K_2\overrightarrow{\delta}_X) - \frac{B_8}{\Delta Z^2} - \frac{B_9}{\Delta X\Delta Z} - \frac{B_{11}}{\Delta Z}\right) G_{i,j}^{n+1} = \alpha\omega L(\phi_{i,j}^n) \tag{28}$$

$$\left(\alpha - A_{3c}\frac{\overleftarrow{\delta}_Y\overrightarrow{\delta}_Y}{\Delta Y^2} + (A_{3u}+B_3)\frac{\overleftarrow{\delta}_Y}{\Delta Y^2} - B_{10}\frac{\overleftarrow{\delta}_Y}{\Delta Y\Delta Z}\right) \Delta_{i,j}^{n+1} = G_{i,j}^{n+1} \cdot$$

It was found that the off diagonal terms of the $F_{XZ}$ derivative could be included in the subsonic crossflow region but not in the supersonic region leading to the following for the $\delta_{XZ}$ operator for U > 0, or

$$\overleftarrow{\delta}_{XZ} = ( )^{n+1}_{i,j,k} - ( )^{n}_{i-1,j,k} - ( )_{i,j,k-1} + ( )_{i-1,j,k-1}$$

$$\overrightarrow{\delta}_{XZ} = ( )^{n+1}_{i+1,j,k} - ( )^{n}_{i,j,k} - ( )_{i+1,j,k-1} + ( )_{i,j,k} \qquad (29)$$

where the subscript K refers to the present R station and K-1 refers to the known values of the potential at the previous station. Hence, care must be taken to preserve the proper balance of new and old values of the potential.

Because of the split nature of the governing equation and R dependence, the AF1Z scheme was found to converge most reliably and optimally if the acceleration parameter $\alpha$ was scaled with R, or

$$\alpha_{min} \sim \alpha_{min} \quad \frac{1}{\Delta X}, \frac{1}{\Delta Y} \quad (1 + R)$$

$$\alpha_{max} \sim \alpha_{max} \quad \frac{1}{\Delta X^2}, \frac{1}{\Delta Y^2} (1 + R) \; . \qquad (30)$$

Hence, the acceleration parameter variation reduces to the conical value at R = 0 and increases linearly with R as the marching solutions are obtained. Since the nonconical coefficients are scaled with R, the acceleration parameters must also be scaled. This scaling will cause the retention of approximately the same convergence rate for a body of length unity versus an arbitrary dimensional length.

### 2.3.1 Three-dimensional Applications of the AF1Z Scheme

Although it is impossible to test the AF1Z scheme for all possible situations, test case computations were carried out on a variety of arbitrary wings and bodies. The following test cases were computed with the bow shock fit option.

Figure 11 illustrates the convergence history of the first case of a highly swept delta wing at $M_\infty = 1.80$, $\alpha = 0°$. The wing geometry consists of a

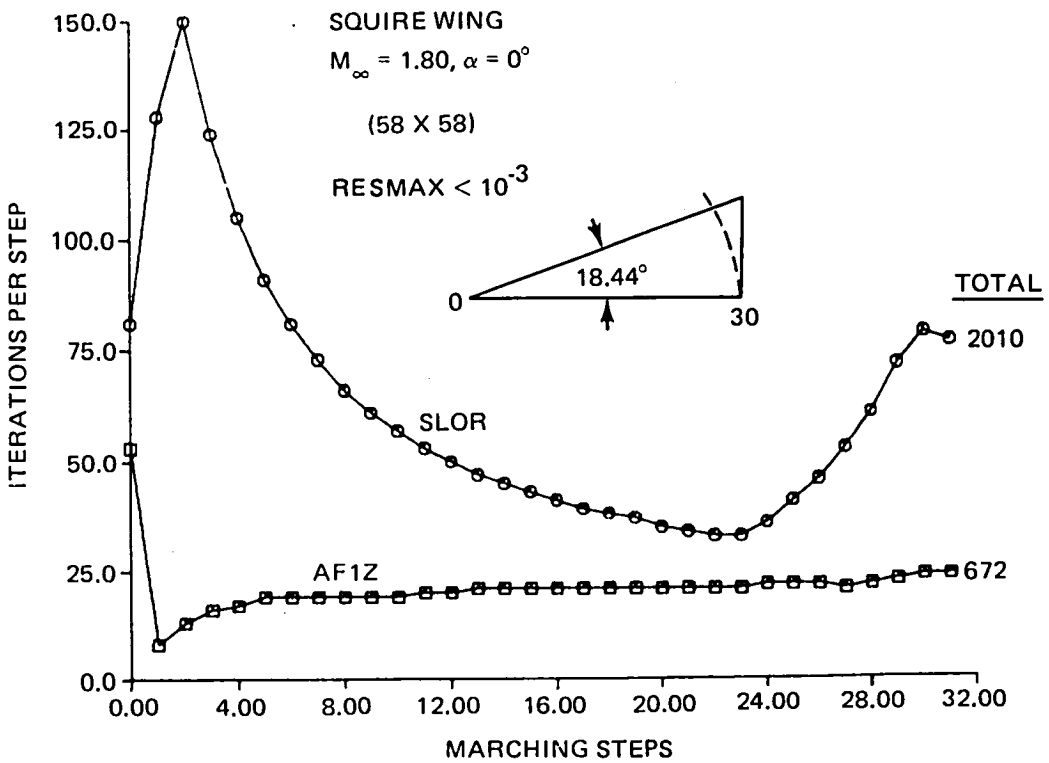


1264-011(T)

**Fig. 11 Squire Wing Computation, AF1Z vs SLOR (BSF)**

parabolic centerline thickness distribution with elliptic spanwise cross sections. As is the case for most three-dimensional wings, the geometry commences near the apex with a thick (e.g., 3:1 major to minor axis ratio) cross section which becomes thin and eventually approaches a flat plate cross section at the trailing edge. Figure 11 shows the number of iterations required per marching step to reduce the maximum residual to 10-3 (i.e., a minimum of four orders of magnitude) for the SLOR and AF1Z schemes. Step 0 refers to the conical or R = 0 solution required to start the computation. Fitting the bow shock as the outer boundary reduces the internal flow field computation to an elliptic problem if an embedded supersonic crossflow region does not form. For this case, the entire flow field was elliptic. Mesh refinement is used only at the conical station, and the marching proceeds on the fine mesh using the previous station solution as an initial guess. The iterations at step 0 reflect only the fine grid convergence. The AF1Z scheme shows large gains for the initial steps. At the initial steps, the geometry changes most rapidly. The AF1Z gains taper off as the cross section becomes quite thin. The SLOR scheme has some difficulty computing the latter stations in comparison with the AF1Z scheme. Step 30 corresponds to the centerline trailing edge. The calculation is taken beyond the trailing edge in order to compute the entire wing. The wake is assumed to be a flat plate, which in this case is an exact assumption. The total iterations for the run are also shown in Fig. 11. The SLOR computation took 2010 fine grid iterations, and the AF1Z scheme required only 672 iterations, producing an overall factor of three reduction in iterations. The actual computation time, which includes geometry and mesh generation, was reduced by a factor of two.

The next case, shown in Fig. 12, is for a 67° sweep angle arrow wing at $M_\infty = 1.75$, $\alpha = 5°$. The geometry consists of a symmetrical, NACA 4% thick, four-digit airfoil imposed chordwise on the wing. The wake is approximated as a flat plate. In this calculation, the flow field very quickly becomes supercritical at R = 3 or STEP 4. The same trends apply for this case except that the SLOR scheme does not have any rise in iterations near the trailing edge of the wing. The interesting aspect of the AF1Z scheme is that the number of nonconical iterations required per step is relatively constant and independent of the geometry variation. Almost a factor of three reduction in iterations is again achieved by the AF1Z scheme corresponding to a factor of two in running time. Hence, the appearance of supercritical crossflow and a

crossflow shock does not seem to deteriorate the AF1Z scheme significantly. In addition, aft of the trailing edge, the crossflow shock merges with the trailing edge shock.

Another case, shown in Fig. 13, is for a realistic, supersonic maneuver, demonstration wing designed with the aid of NCOREL[18] and tested by NASA Langley. Details of this wing can be found in Ref. 19. This wing has a variable sweep leading and trailing edge. The leading edge planform angle varies from 25° to 33°. The wing also has significant twist and camber. Figure 13 shows the convergence histories for the two schemes at $M_\infty = 1.62$ and $\alpha = 14°$. The wake is approximated by a flat plate extension of the wing spanwise camberline. For this wing, supercritical flow also appears at R = 3 or STEP 4. Similar trends apply for this wing except that the AF1Z scheme gains are reduced aft of the trailing edge of the wing. The overall reduction in iterations is similar, being almost a factor of three and corresponding to a factor of two reduction in running time.

All of the previous cases were run on a relatively fine grid (58 x 58). Figure 14 shows the iteration ratio of the SLOR to AF1Z scheme for several grids, corresponding to the DEMO wing computation of Fig. 13. The AF1Z scheme performs almost as well on the cruder meshes as on the finest mesh, retaining between a factor of two to three reduction in number of iterations. Figure 14 does indicate that the performance gain will increase on the finer grids.

The AF1Z scheme performs well for wing computations. The next set of cases will test the scheme for body computations. Figure 15 shows the convergence history for an axisymmetric circular arc cylinder body at $M_\infty = 1.60$, $\alpha = 10°$ on a 58 x 58 mesh. For this case, the crossflow is subsonic along the entire length of the body and, hence, shockless. The AF1Z scheme performs nicely by reducing the number of iterations by a factor of four.

Figures 16 to 18 show another set of computations for a more difficult body shape: an elliptic cross section (3:1 axis ratio) with a Haacke-Adams area distribution. Figure 16 shows the computations at $M_\infty = 1.60$, $\alpha = 5°$ on a 58 x 58 mesh. Better than a factor of four reduction in number of iterations is achieved for this condition. Figure 17 shows a higher Mach number case ($M_\infty = 2$, $\alpha = 5°$) for the same body. For this condition, just under a factor of three reduction was achieved. Both schemes seem to have difficulty in the supercritical crossflow region that commences at around 20 in the marching

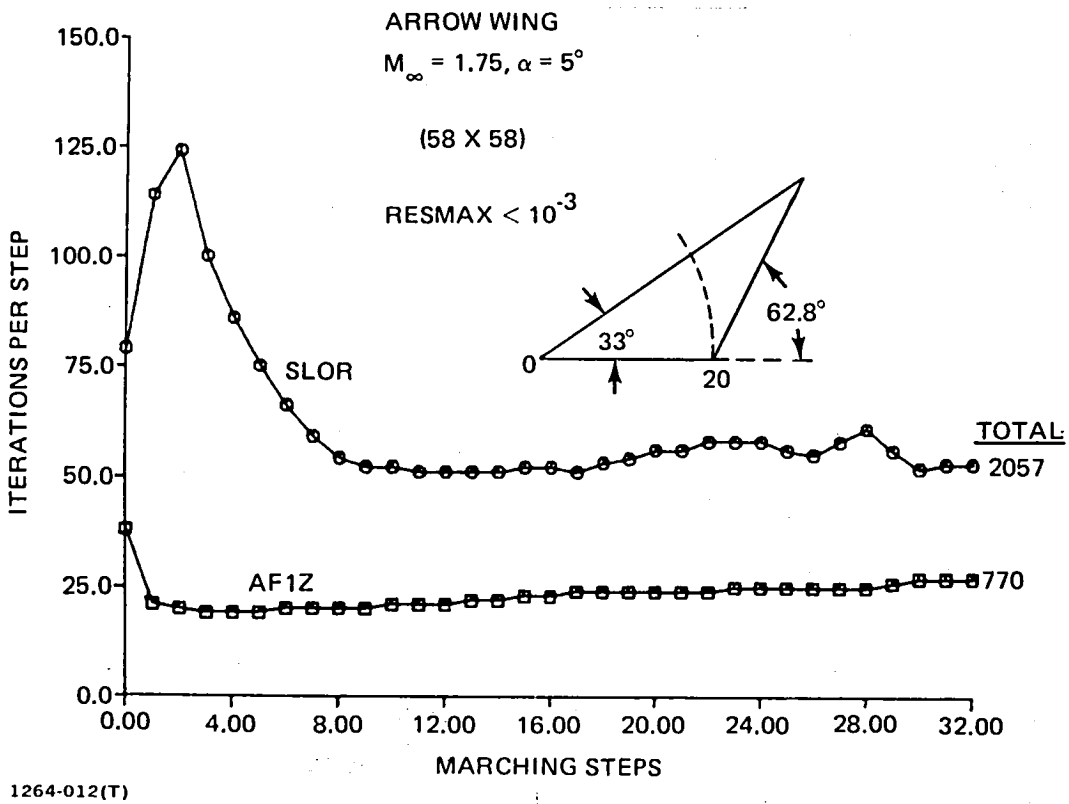


Fig. 12 Arrow Wing Computation, AF1Z vs SLOR (BSF)

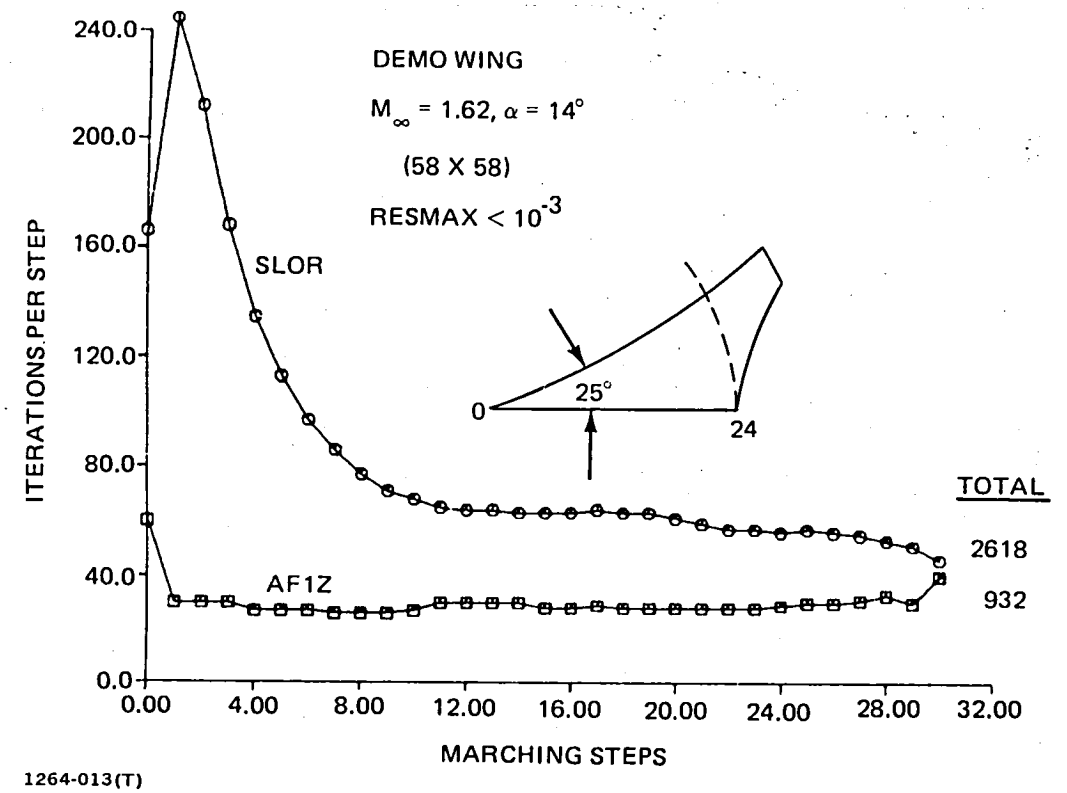


Fig. 13 Demonstration Wing Computation, AF1Z vs SLOR (BSF)

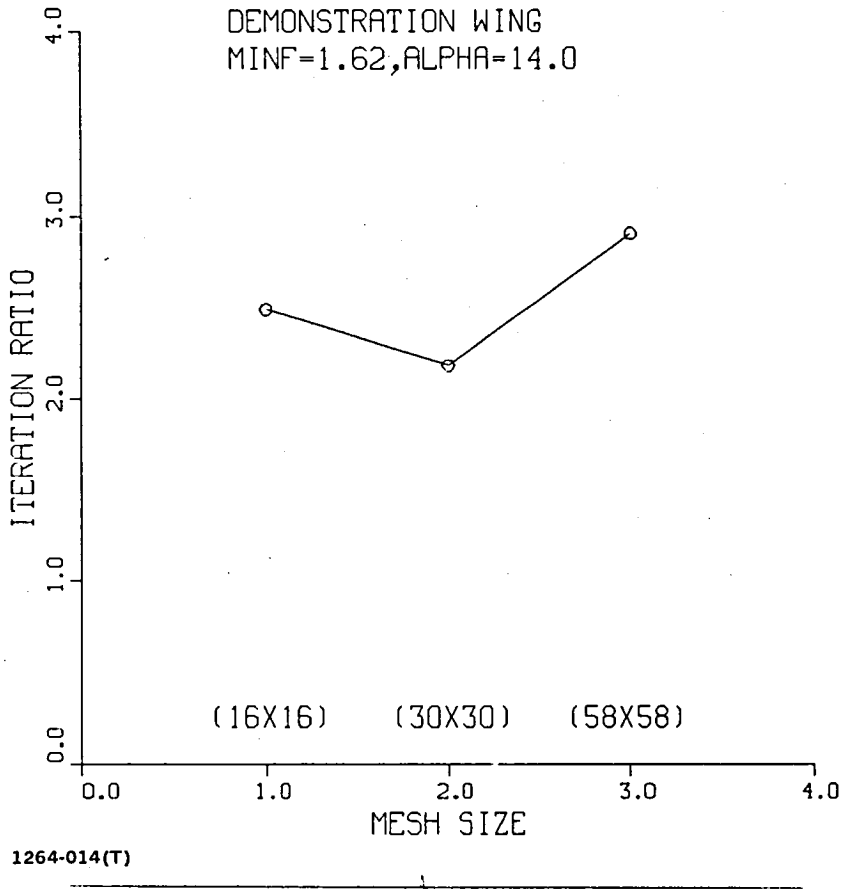


**Fig. 14 SLOR vs AF1Z Convergence Ratio for Varying Mesh Sizes**

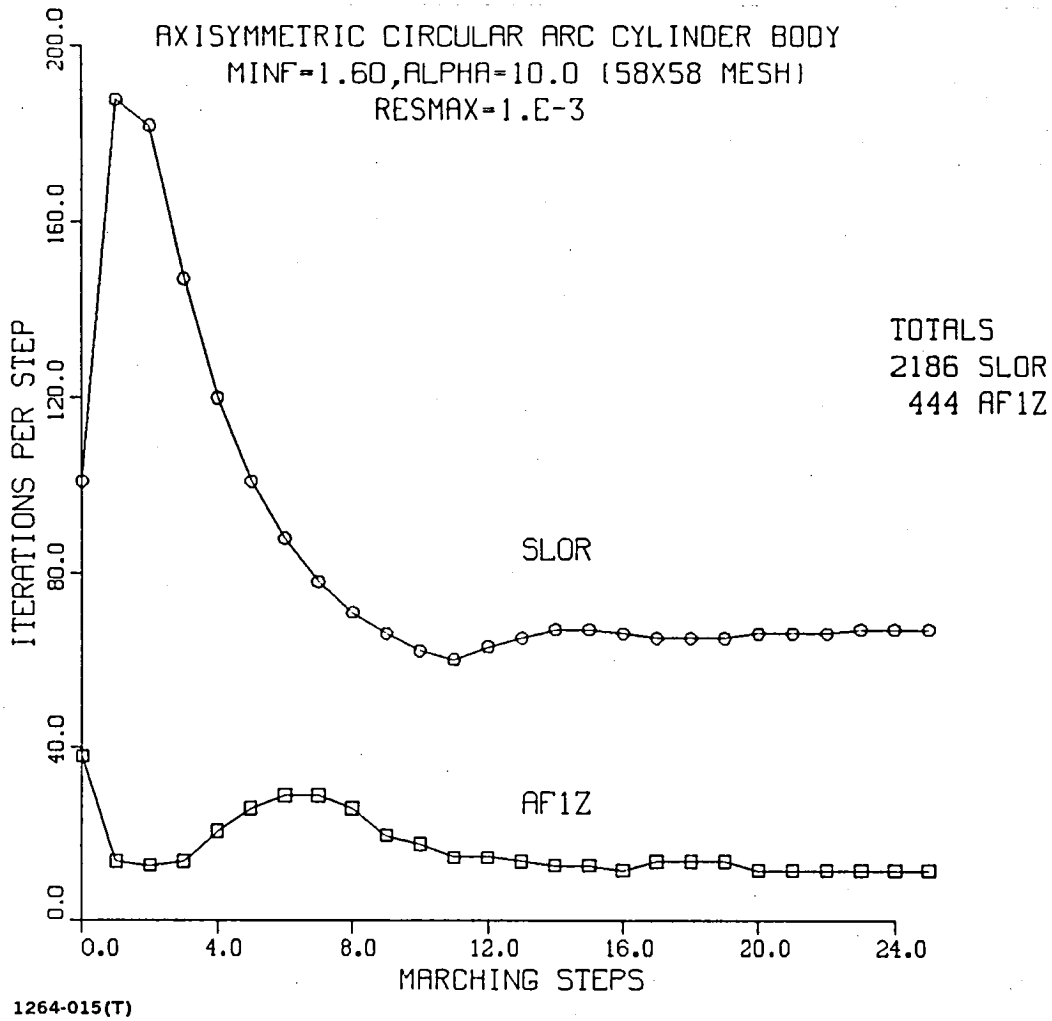


**Fig. 15 Axisymmetric Circular Arc-cylinder Body Computation at $M_\infty = 1.60$, $\alpha = 10^\circ$, AF1Z vs SLOR**

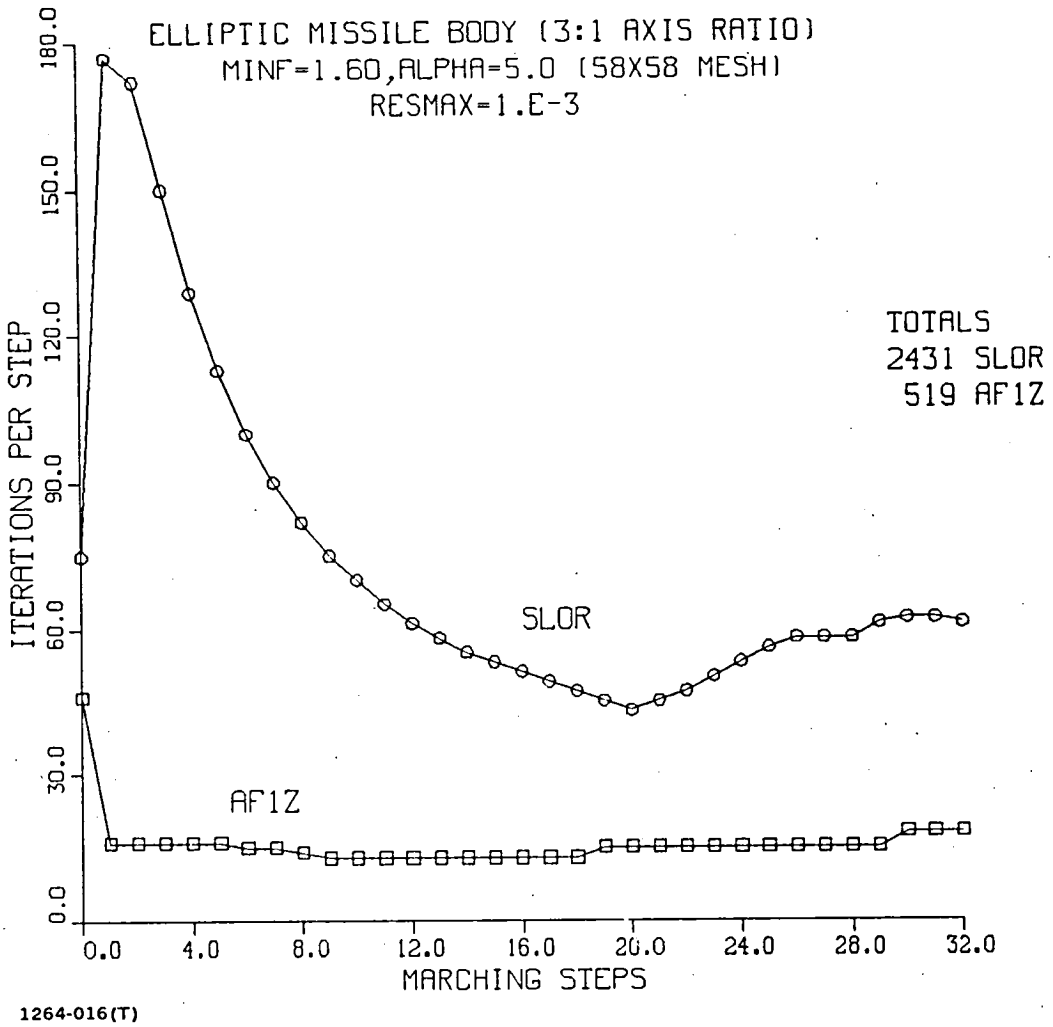


**Fig. 16 Elliptic Missile Body Computation at $M_\infty = 1.60$, $\alpha = 5^\circ$, AF1Z vs SLOR**

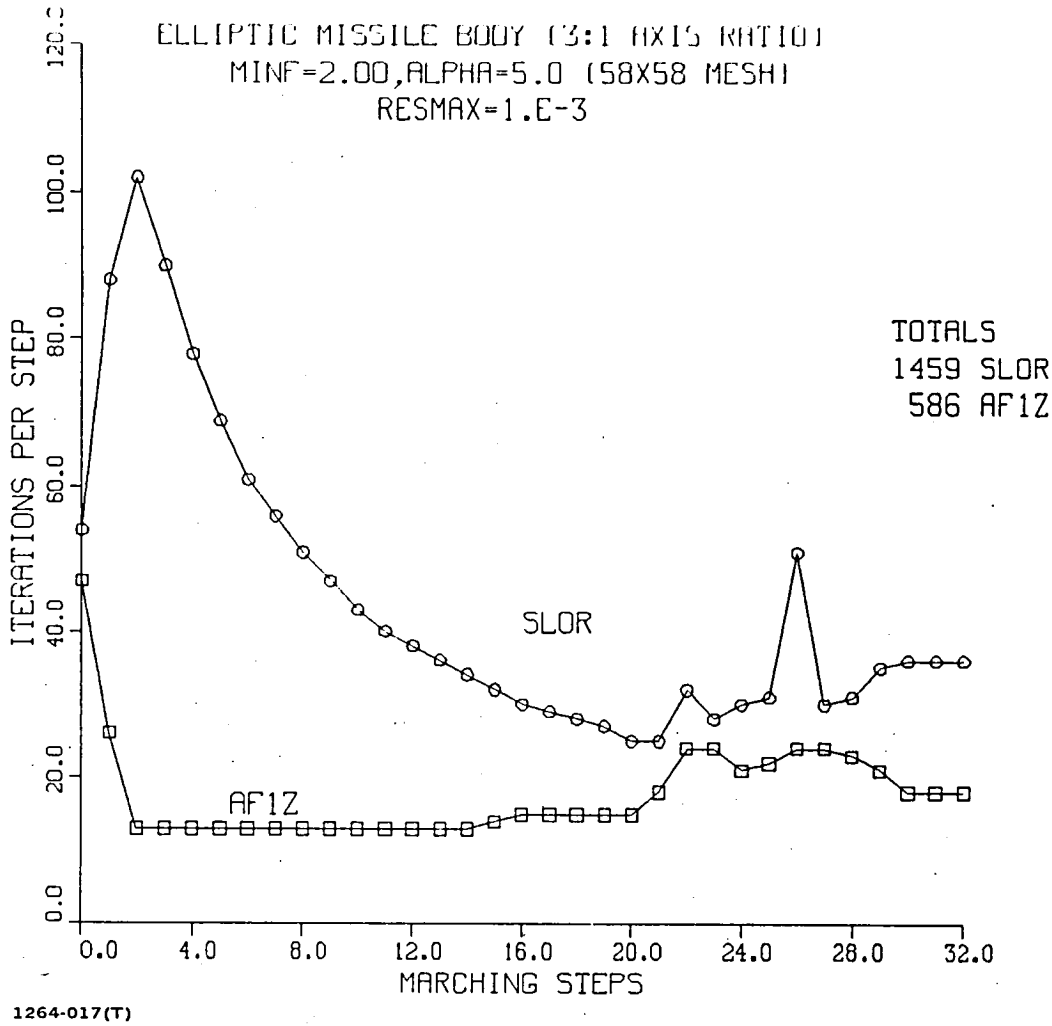


**Fig. 17 Elliptic Missile Body Computation at $M_\infty = 2.0$, $\alpha = 5^\circ$, AF1Z vs SLOR**

steps. Figure 18 shows an even more extreme and difficult condition to compute, $M_\infty = 2$, $\alpha = 10°$. For this condition, the crossflow is supersonic at the conical start, with the crossflow shock becoming increasingly stronger toward the aft end of the body. The AF1Z scheme performs well initially, but both schemes begin to have difficulty towards the aft end of the body. Not quite a factor of two reduction in iterations is achieved.

In summary, the AF1Z scheme seems to be reasonably reliable and can be made to run faster than the SLOR scheme over a wide range of configurations. Even for difficult bow shock fit computations, the AF1Z will run faster although the gains achieved are not as great as at the lower Mach number conditions. It must be mentioned that the effect of the AF parameters was not intensively explored for the previous computations and, hence, a more thorough study of these parameters might yield greater reductions.

## 2.4 PARAMETER SELECTION

Although it is impossible to test the AF1Z scheme for all possible situations, test case computations were carried out on a variety of arbitrary wings and bodies. The $\alpha$ variation that was found to work best in a variety of cases was

$$\alpha_{max} = \frac{2}{\Delta Y^2}(1 + R)$$

$$\alpha_{min} = \frac{1}{\Delta X}(1 + R) \qquad (31)$$

where the cycles between $\alpha_{max}$ and $\alpha_{min}$ are two or three for crude to medium meshes (16 x 16 → 48 x 48) and four for finer meshes (58 x 58 and above). The exception to this rule is for more difficult bow shock fit cases at high Mach number or incidence. For these cases, the alpha range of Eq (31) should be raised. For example, in Eq (31), $A_{min} = 1$, $A_{max} = 2$; these values might be raised to $A_{min} = 2$, $A_{max} = 4$ for the crude mesh to get the bow shock fit computation started. In addition, the number of cycles ITMAX might be raised to 6 on the crude mesh. After the crude mesh is successfully computed, the default values can probably be used on the finer and nonconical meshes.

The AF1Z scheme can be run with a relaxation factor ($\omega$) for the residual up to 1.7. Since the AF1Z scheme converges faster than the SLOR scheme, the

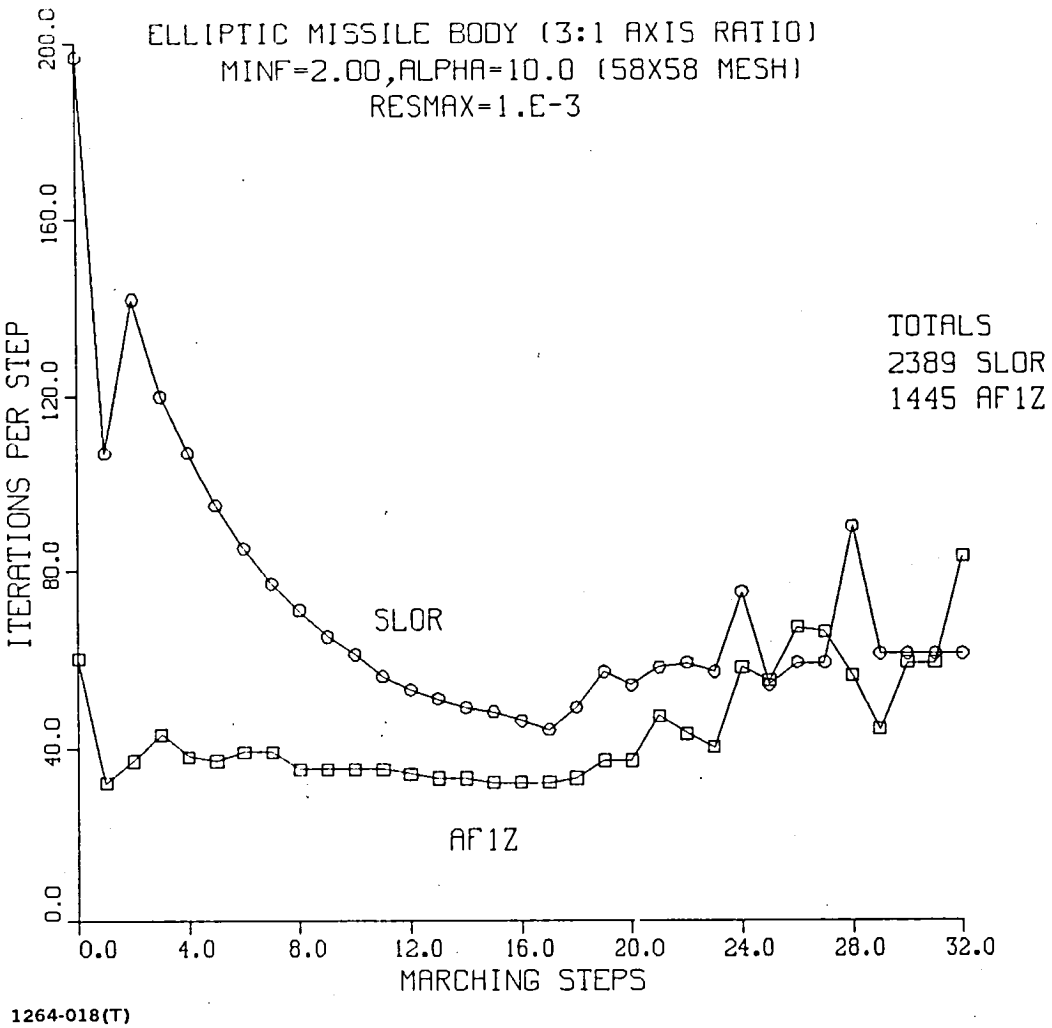


**Fig. 18 Elliptic Missile Body Computation at $M_\infty = 2.0$, $\alpha = 10^\circ$, AF1Z vs SLOR**

bow shock relaxation ($\omega_S$) factors can also be increased both at the conical start and at the nonconical stations. Typically, $\omega_S$ = 3.0 was used at the nonconical stations. The temporal artificial viscosity or damping terms controlled by the parameter EST are also included in the AF1Z scheme. For most cases, with the exception of difficult cases with strong embedded shocks, the AF1Z sheme can be run with the EST parameter set to zero. For cases that require damping, the value of EST should be set at very small values (e.g., $-0.001 > EST > -0.10$). For most cases -0.01 or -0.001 is sufficient. Nonzero values of EST in the AF1Z scheme degrade the convergence considerably and should be avoided.

# 3. WAKE FLOWS

In general, wake flows are characterized by a discontinuity or slip in velocity with a continuity in pressure. In potential flows, a jump in potential is prescribed across the wake which accounts for the circulation or lift about the wing or airfoil. In two-dimensional potential flows the velocity is continuous, but the potential has a constant jump across the wake streamline. Matching pressures at the trailing edge in the wake cut also impose a Kutta condition and cause the wake streamline to leave the trailing edge in a direction along the trailing edge bisector. For the Euler equations the situation can be different because of entropy losses across shock waves. If shock waves of different strengths exist on the upper and lower surfaces of an airfoil a slip line with a jump in velocity will arise in the wake due to the differences in total pressure and entropy along the upper and lower surface streamlines.

On the other hand, in three-dimensional flows, contact discontinuities arise in the wake for both Euler and potential flow formulations. In addition, in three dimensions, depending on the trailing edge geometry and flow conditions (e.g., cusped or finite angle), the trailing edge streamline will leave tangentially to one of the surfaces or at the mean angle of the trailing edge[20]. In potential flows, the slip in velocity is due to a discontinuity in the direction of the total velocity vector at the wake surface. The magnitude of the velocity vector must match on the wake to impose the Kutta condition and continuity of pressure along the wake surface. The discontinuous direction of the wake surface total velocity vector causes at least two of the three components of velocity to be discontinuous or to have a slip. For the most part, in three-dimensional transonic flows, the wake is treated in a similar fashion to its two-dimensional counterpart. The jump in potential for a particular airfoil section is assumed constant to downstream infinity. This approximation matches the longitudinal or axial velocity. A continuous velocity is also imposed through the wake surface. The spanwise velocity on the wake surface is not matched and is just proportional to the variation in circulation or lift and, hence, to the variation in the spanwise potential jump for each airfoil section. Hence, the magnitude of the total velocity vector and

resultant pressure is only approximately matched on the wake surface. This is a good approximation for wings that are not highly swept or tapered. A similar wake treatment is used by Shanker, et al[21] for three-dimensional supersonic flows.

Up to the present time, no attempt had been made to model the wake in NCOREL, and a flat plate treatment had been utilized. The successful application of NCOREL to three-dimensional wings and bodies suggested that a wake treatment might further extend its applicability to wing-body and more complex configurations.

In the present formulation, the wake is also modeled approximately as a planar cut in three dimensions. Here, the Kutta condition at the trailing edge and the continuity of pressure on the wake surface are imposed exactly. Therefore, as distinct from other treatments, the behavior for the jump in potential is not prescribed a priori, but rather computed at every point on the wake surface. Initially, a conical wake problem will be discussed along with some special aspects concerning this problem. These basic techniques are then readily extendable to the fully three-dimensional flow about wings and wing-body configurations.

## 3.1 CONICAL WAKE PROBLEM

A conical wake problem was devised to test the basic numerics required to solve the fully three-dimensional supersonic wake flow. In this problem, sketched in Fig. 19a, the wing cross section and wake surface share a common apex. This problem has already been considered by J.H.B. Smith[(22)], where some general behavior was postulated theoretically and will be discussed in a later section.

The wake is modeled as a planar surface cut of infinitesimal thickness. The wing cross section and wake cut (see Fig. 19b) are then mapped to a near circle ($\rho$, $\theta$, R) using conformal mappings and further sheared to a computational domain (X, Y, Z).

Flow tangency is obtained by using a dummy row of grid points around the body whose values are obtained by imposing the vanishing of the normal velocity through the $F_Y$ derivative. For positive angle of attack, the flow on the lower surface of the wake cut is computed with the boundary condition that the velocity component through the wake cut is continuous.

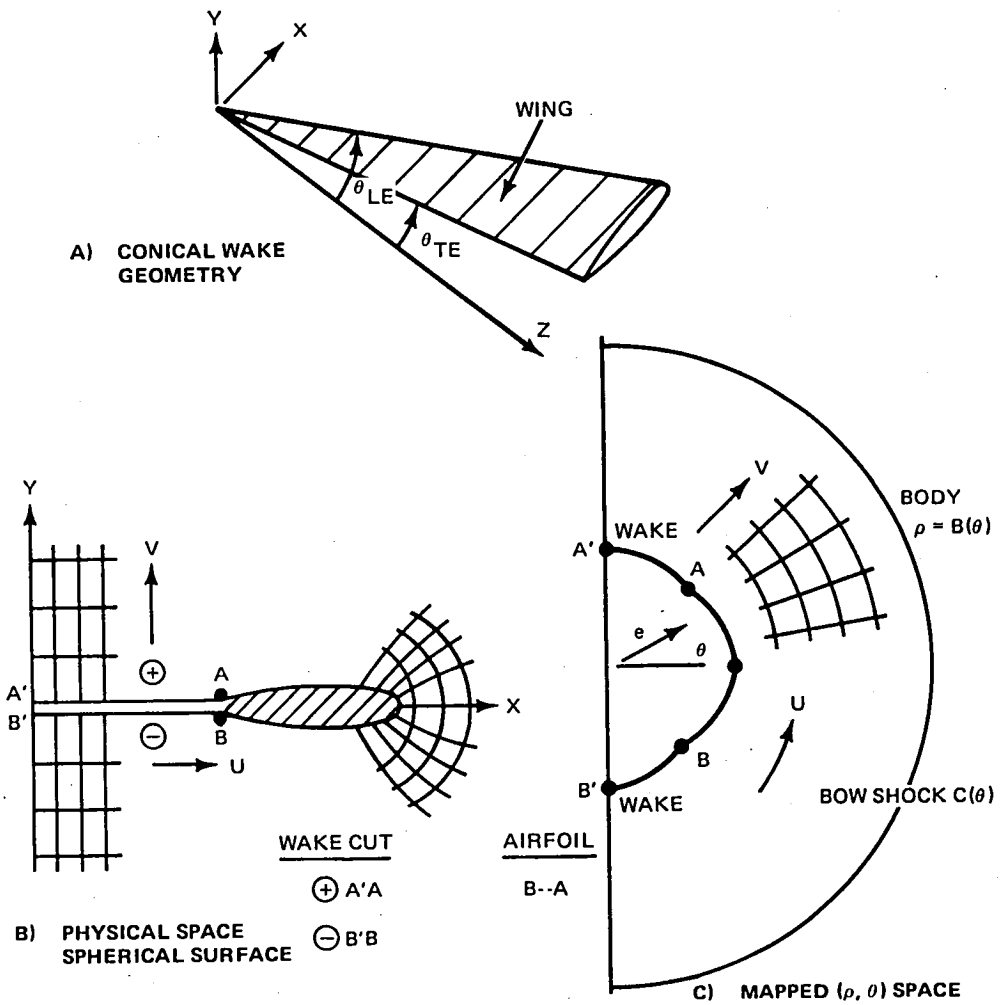


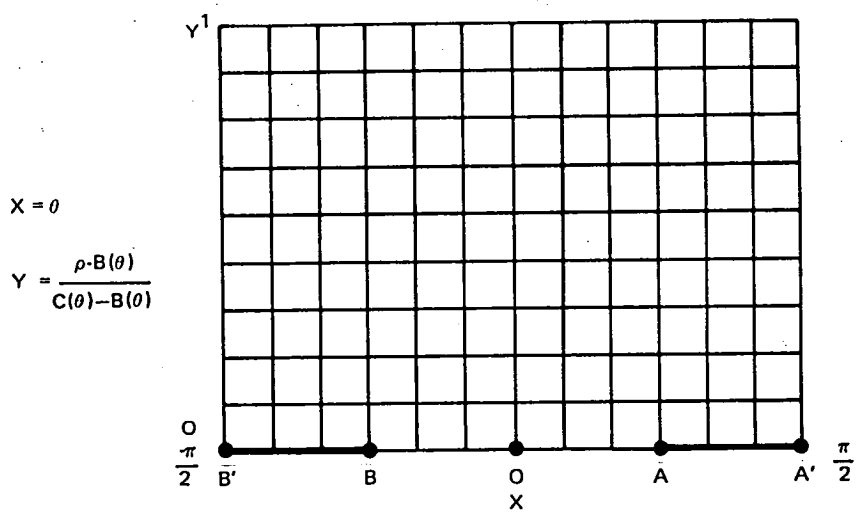


1264-019(T)

**Fig. 19 Conical Wake Problem**

The velocity components for conical flow are defined in the mapped coordinate system ($\rho$, $\theta$, R) as:

$$U = \frac{1}{\rho H} F_\theta + u_\infty = \frac{1}{\rho H} (F_x X_\theta + F_y Y_\theta) + u_\infty$$

$$V = \frac{1}{H} F_\rho + v_\infty = \frac{1}{H} F_y Y_\rho + v_\infty \qquad (32)$$

$$W = F + w_\infty$$

where $\phi = RF(\rho,\theta)$ and U is circumferential and W is the radial velocity component. The airfoil and wake cut are defined as Y = 0 in the computational domain. If a variable jump in potential exists along the wake segment, in general, the U velocity will reflect this discontinuity or slip, and the V velocity (which does not have $F_x$ in its definition) will be constrained to be continuous.

For V to be continuous, the condition that

$$V_w^- = -V_w^+ \qquad (33)$$

must be imposed on the wake cut where the change in sign reflects the opposite sense of the mapped cylindrical coordinate system. This condition (33) further reduces to

$$\left(\frac{F_y Y_\rho}{H}\right)^- = -\left(\frac{F_y Y_\rho}{H}\right)^+ \qquad (34)$$

since the corresponding upper and lower wake surface points map to the same point in physical space yielding the same freestream velocity. The wake condition (34) is imposed by computing the value of $F_Y$ in a one-sided fashion on the upper wake cut and is then used as the boundary condition on the lower wake cut. The computational method proceeds by computing on lines X = constant commencing at the lower symmetry plane and sweeping around to the upper symmetry plane. On the lower wake cut, the governing full potential equation is satisfied subject to condition (33). On the wing surface, flow tangency is satisfied. Both conditions use a Neumann boundary condition given by the dummy row of potentials. On the upper wake cut, the full potential

equation is not satisfied. Instead, a jump in potential is assumed to exist at every point on the upper wake cut as

$$F_w^+ = F_w^- + \Delta F(\theta_w) \ .$$

The upper wake cut X = constant lines are then solved as a Dirichlet problem once a jump in potential has been imposed.

In summary, the X = constant lines emanating from the lower wake cut are solved by using a Neumann type boundary condition obtained for condition (33) where $V_w^+$ is derived from a one-sided difference in the upper wake plane. Hence, communication across the wake exists without explicitly differencing across the wake cut, thus eliminating the necessity for interpolation. An equation for the jump in potential is now needed that matches the pressures all along the wake cut. For potential flows, it is a sufficient condition to match the total speed along the wake cut for the pressures to match. Equality of total speed can be expressed by the equation

$$\bar{U}(U_{w+}-U_{w-}) + \bar{V}(V_{w+}-V_{w-}) + \bar{W}(W_{w+}-W_{w-}) = 0 \qquad (35)$$

where

$$\bar{U} = U_{w+} + U_{w-}$$

$$\bar{V} = V_{w+} + V_{w-}$$

$$\bar{W} = W_{w+} + W_{w-} \ .$$

Some interesting aspects of the conical wake problem can be uncovered by inspection of Eq (35). At the symmetry planes $U_{w\pm} = 0$ and $V_{w+} = -V_{w-}$; Eq (35) then reduces to

$$W_{w+} = W_{w-} \Big|_{X = \pm \pi/2} \qquad (36)$$

which implies, given the definition (32), that

$$\Delta F_w(x = \pm \frac{\pi}{2}) = F_{w+} - F_{w-} = 0 \ . \qquad (37)$$

Hence, in the conical wake problem, for the pressures to be matched across the wake cut at the symmetry plane, the jump in potential must vanish. Thus, at the trailing edge, the wake initially reflects the jump in potential coming off the trailing edge of the airfoil, and eventually the jump must vanish at the symmetry plane in order for the pressures to match.

In practice, Eq (35) can be implemented recursively by solving for $\Delta F$ in terms of the U, V and average velocities on the wake cut. The new value of the jump in potential is computed based on old values of the velocity and is underrelaxed until the full potential equation, flow tangency, and conditions (33) and (35) are all satisfied.

Figure 20a shows the conical pressure solution on an (82 x 58) mesh about the airfoil and wake cut at $M_\infty = 2.0$, $\alpha = 5°$ and $\theta_{LE} = 20°$, $\theta_{TE} = 10°$. A crossflow shock occurs on the upper surface of the airfoil. The pressures match smoothly at the subsonic trailing edge. A grid point is not situated exactly at the trailing edge. A slight expansion occurs near the symmetry plane along the wake cut. Figure 20b shows the corresponding potential distribution about the airfoil along with the jump in potential computed for the wake cut. The jump in potential along the wake cut is relatively linear except near the symmetry plane. Figure 20c shows the overall computed isobar pattern. Figure 20d shows the streamline pattern in the vicinity of the airfoil. The trailing edge streamline leaves the airfoil smoothly, and it appears to leave tangentially to the lower surface. The streamlines crossing the wake cut are discontinuous due to the slip in velocity on the wake surface. An interesting feature of this computation is that the wake circumferential V velocities are negative along a portion of the upper wake cut near the symmetry plane. The wake streamline terminates at the symmetry plane as a nodal or vortical singularity.

Figure 21 shows another computation for a thinner airfoil section at $M_\infty = 1.7$, $\alpha = 5°$ with $\theta_{LE} = 30°$ and $\theta_{TE} = 20°$. This computation behaves in a similar fashion exhibiting a subsonic trailing edge behavior. For the trailing edge to be supersonic in the conical wake problem, the crossflow Mach number at the trailing edge would have to be supersonic. The author has not been able to find a conical situation in which a supersonic crossflow exists at the trailing edge.

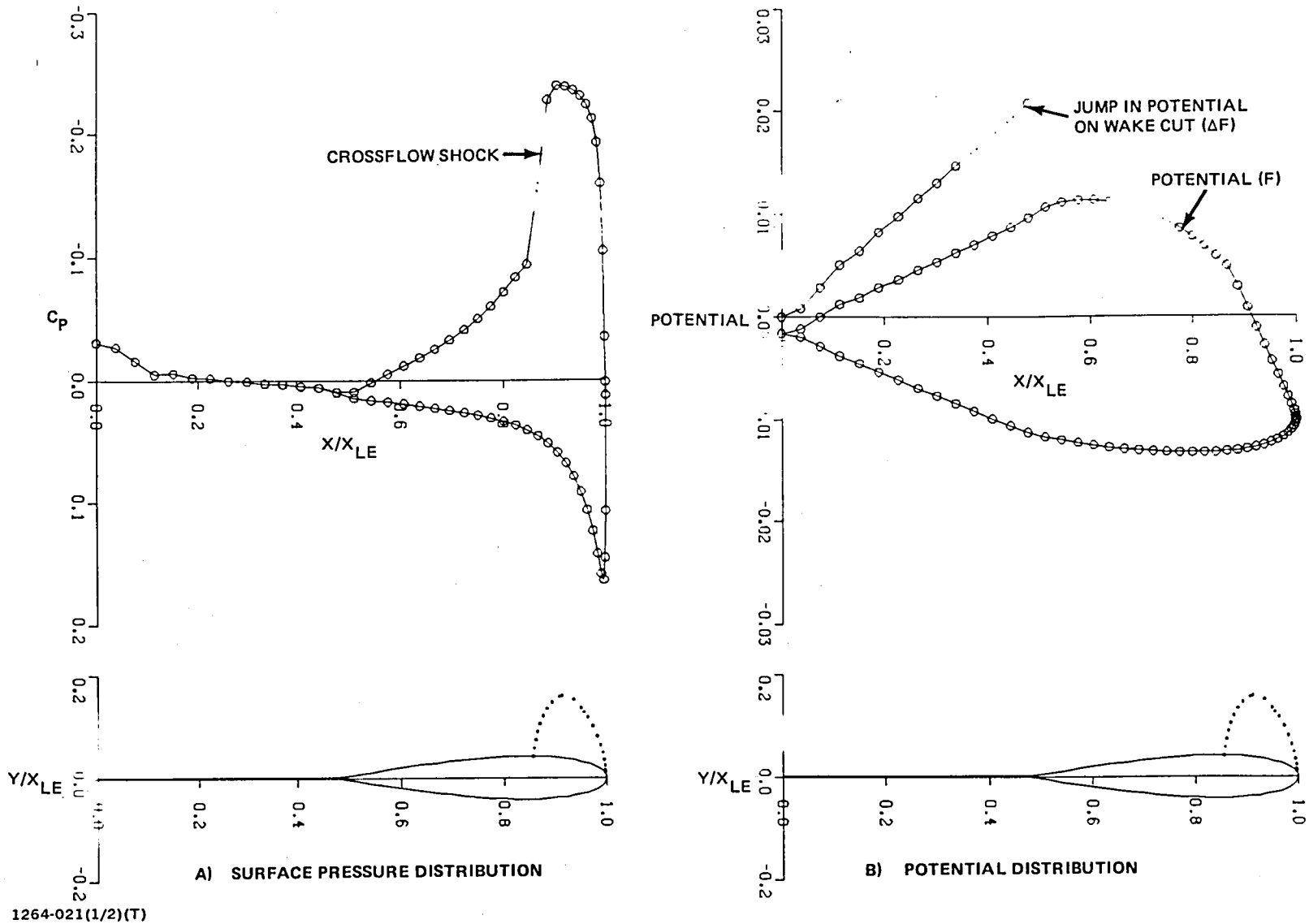


Fig. 20 Conical Wake Solution for $M_\infty = 2.0$, $\alpha = 5^\circ$ ($\theta_{LE} = 20^\circ$, $\theta_{TE} = 10^\circ$) (Sheet 1 of 2)

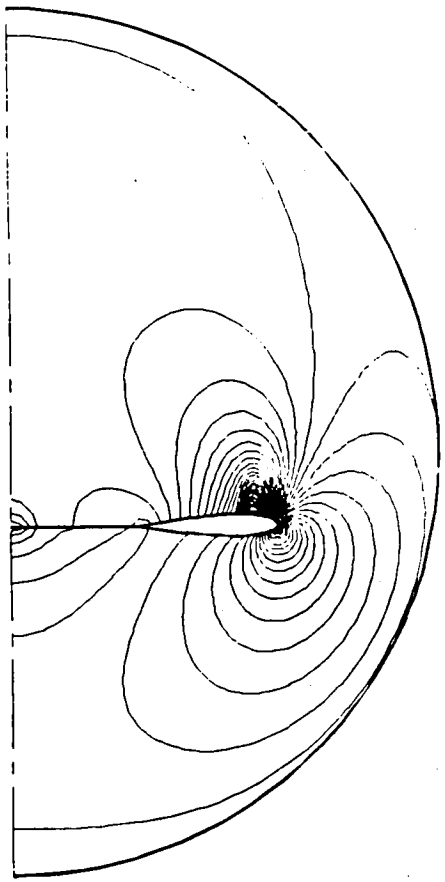

C) ISOBAR PATTERN

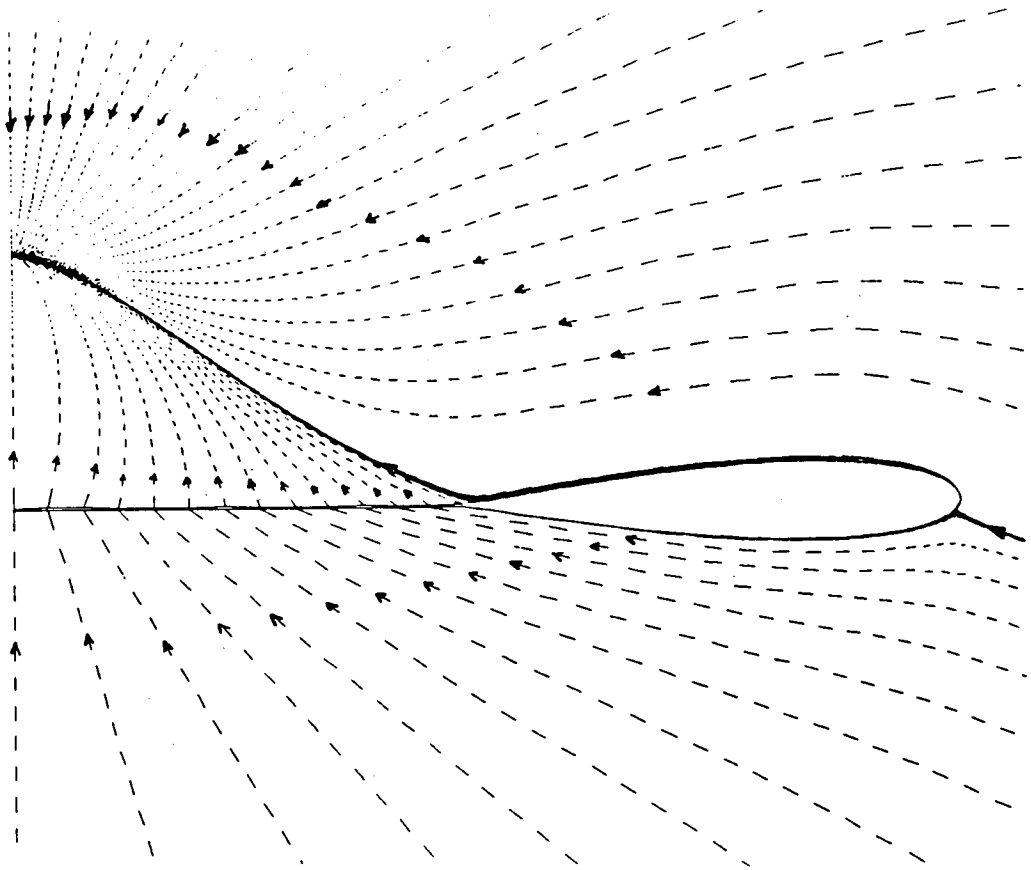

D) ENLARGED VIEW OF CROSSFLOW STREAMLINES

1264-021(2/2)(T)

Fig. 20 Conical Wake Solution for $M_\infty = 2.0$, $\alpha = 5^\circ$ ($\theta_{LE} = 20^\circ$, $\theta_{TE} = 10^\circ$) (Sheet 2 of 2)

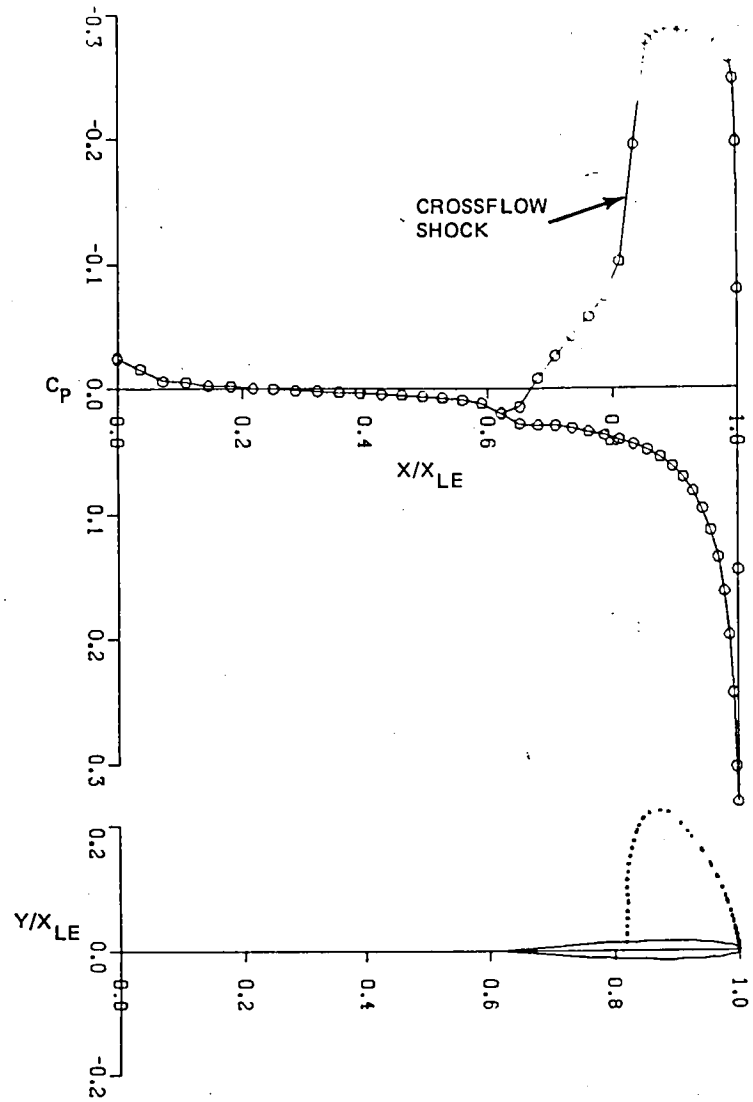


A) SURFACE PRESSURE SOLUTION

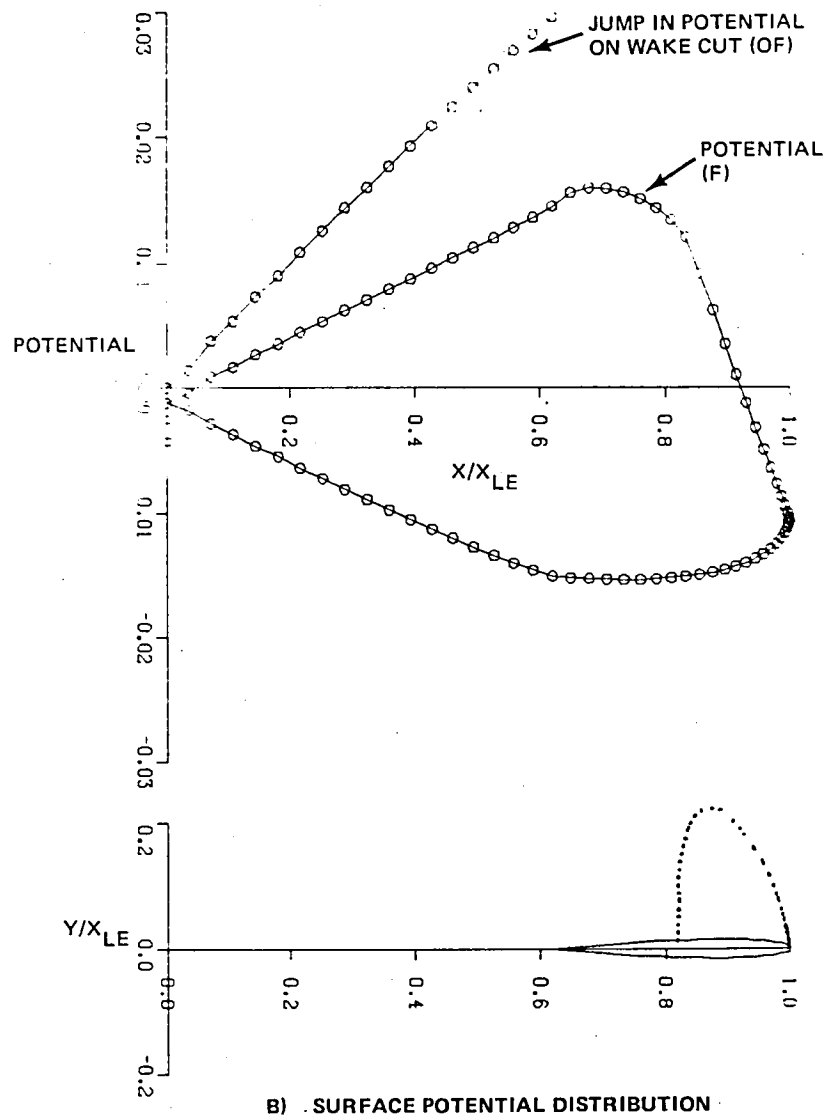


B) SURFACE POTENTIAL DISTRIBUTION

1264-024(T)

Fig. 21 Conical Wake Solution for $M_\infty = 1.70$, $\alpha = 5^\circ$ ($\theta_{LE} = 30^\circ$, $\theta_{TE} = 20^\circ$) (Sheet 1 of 2)

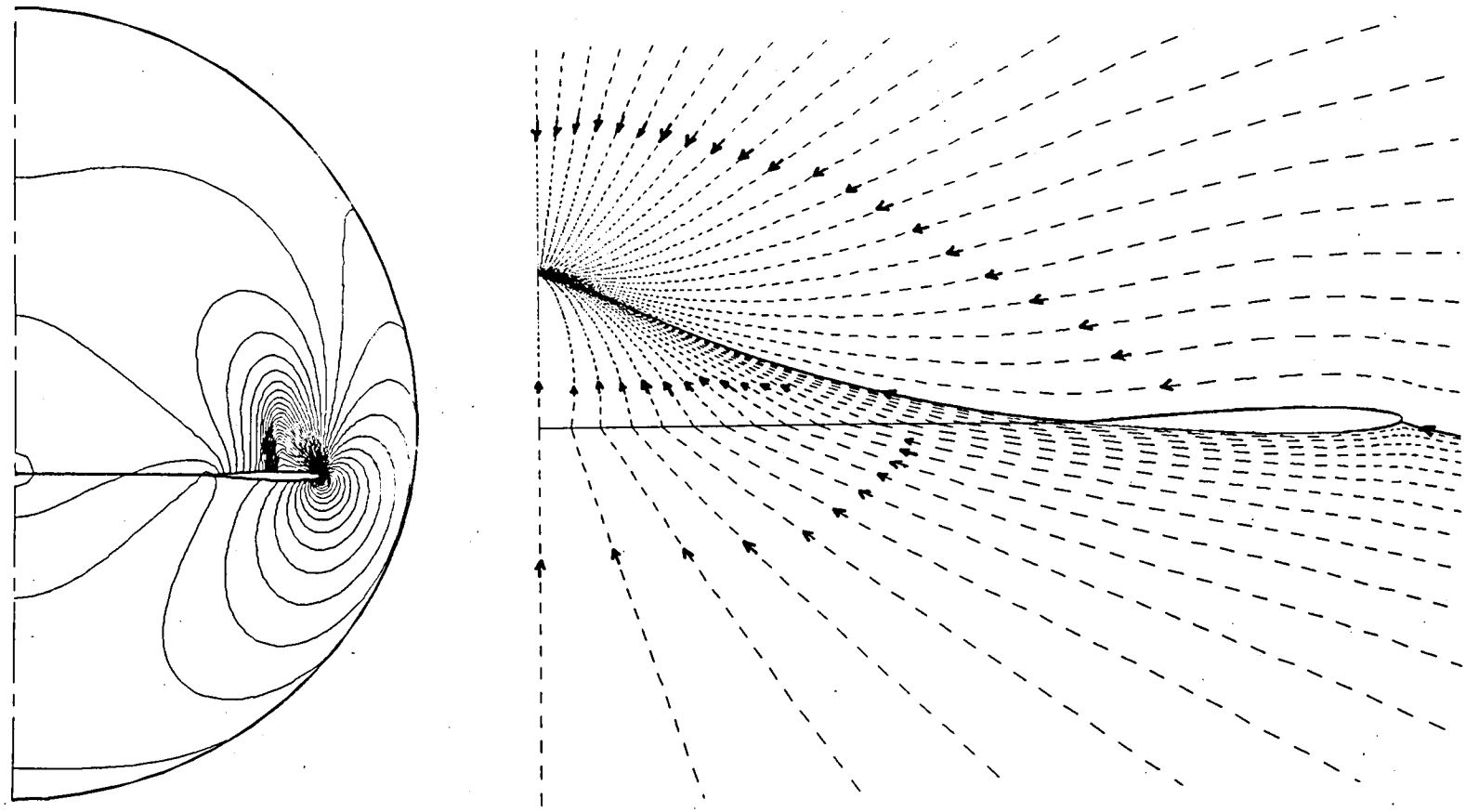

C) ISOBAR PATTERN

D) ENLARGED VIEW OF CROSSFLOW STREAMLINES

1264-024(T)

Fig. 21 Conical Wake Station for $M_\infty = 1.70$, $\alpha = 5^\circ$ ($\theta_{LE} = 30^\circ$, $\theta_{TE} = 20^\circ$) (Sheet 2 of 2)

It was mentioned previously that the conical wake problem has been discussed by J.H.B. Smith[22]. Based on conical flow theory, Smith postulated a crossflow streamline pattern and nodal behavior such as is sketched in Fig. 22. Smith postulated that the wake streamline would roll up into a nodal point. Hence, the vorticity shed by the airfoil would be carried to downstream infinity via the radial velocity at the crossflow nodal or stagnation point. This behavior can not be obtained within the present formulation, but attempts at fitting the conical wake problem indicate that this behavior may occur. The wake could be fit at low angles of attack (e.g., 1° or 2°) but could not be fitted at higher angles of attack, possibly due to the beginning of a rollup behavior.

## 3.2 GENERAL THREE-DIMENSIONAL WAKES

Unlike the conical wake problem, the jump in potential at each point on the wake surface emanating from a three-dimensional wing has as its origin an upstream trailing edge point. Hence, for a lifting wing, in the crossflow plane, a variable jump in potential exists along the wake surface proportional to the circulation about an upstream streamline section. The conical condition that the jump in potential must vanish at the symmetry plane no longer applies to the three-dimensional wing. This condition is alleviated in fully three-dimensional flows because the radial velocity component now contains R derivatives of the potential that relate the jump in potential at the symmetry plane to its upstream origin. The boundary conditions and relationships matching the pressure are the same in the three-dimensional problem as in the conical problem with the exception that the velocities have three dimensional or R derivatives included in their definition.

In some respects, the three-dimensional problem is somewhat simpler to compute since a good initial guess for the jump in potential in the crossflow plane can be generated from the jump in potential across the wake and airfoil section of the previous plane. The variation of the jump in potential along the wake surface is not nearly as large as that which occurs in the conical wake problem. Some underrelaxation must be used in updating the potential jump but the overall rate of convergence is not affected significantly except when a strong shock interaction occurs at the trailing edge.

In general, both subsonic and supersonic trailing edges can occur in the 3-D supersonic wake flow problem. Subsonic trailing edges have local Mach

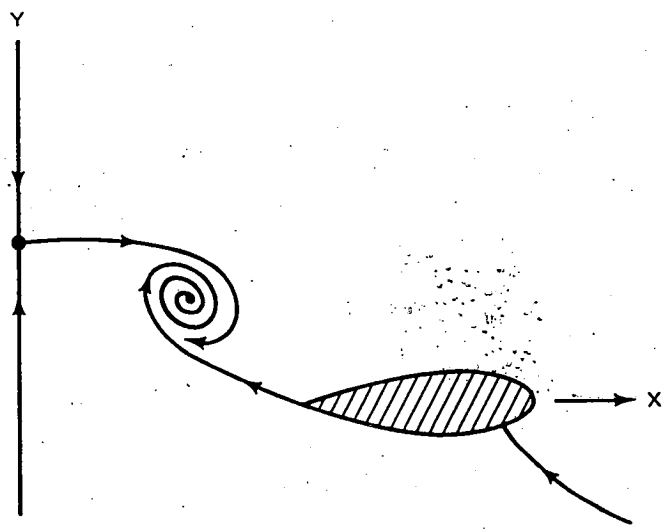


1264-027(T)

**Fig. 22 Conical "Swept Wing" at Incidence (Ref. 6) Postulated by J.H.B. Smith**

numbers in a plane normal to the trailing edge that are less than unity. For this situation, the wake streamline leaves the trailing edge smoothly. When the local normal trailing edge Mach number is supersonic, the airfoil surface streamline will either expand or pass through a shock in satisfying the pressure condition. Depending upon the value of the local normal Mach number at the upper and lower surface trailing edge points, several flow situations can exist. For supersonic trailing edges, these are

- Shock - shock
- Shock - expansion.

A shock or expansion can also occur on one surface in combination with smooth subsonic behavior on the other surface. Figure 23 sketches some of the basic flow situations and their character in the spherical crossflow plane. The trailing edge shock is really a three-dimensional surface which takes a shape similar to that shown in Fig. 23a in the crossflow plane at zero incidence. A crossflow shock can also coexist on the surface of the cross section that will interact with the trailing edge shock(s) and/or expansion. One such complicated interaction is sketched in Fig. 23d from observations of computed crossflow plane isobar patterns. The crossflow shock and trailing edge shock intersect, forming two resultant shocks. The crossflow shock after intersection with the trailing edge shock exists in the flow on the wake cut (i.e., passes through the trailing edge shock) and is attenuated below the wake cut by the lower surface expansion.

### 3.2.1 Symmetric Cross Sectional Geometries

Symmetric geometries were treated initially. The meshes generated for these geometries by NCOREL yield corresponding grid points in the upper and lower surfaces of the wake cut. Hence, no interpolation is required at corresponding upper and lower wake points for the potential or the speed. Figure 24 shows a selected sample of the crossflow plane surface pressure solutions for a symmetric arrow wing with 70° leading edge and 45° trailing edge sweep angles at $M_\infty = 1.75$, $\alpha = 5°$ commencing with the spherical surface that cuts through the centerline trailing edge. Some of the computed wake pressure distributions are compared with the pressure distribu-tions obtained by assuming a flat impermeable plate for the wake. A crossflow shock exists on the upper surface of the airfoil. The upper surface pressures indicate a

A) SYMMETRIC SUPERSONIC TRAILING EDGES ($\alpha = 0°$)

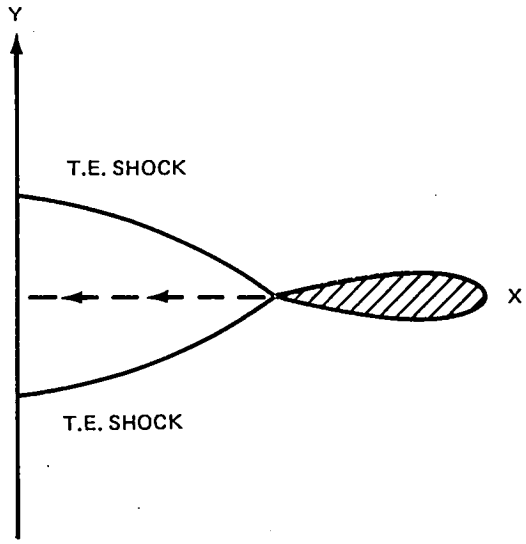


B) SHOCK – SHOCK SUPERSONIC TRAILING EDGES ($\alpha > 0$)

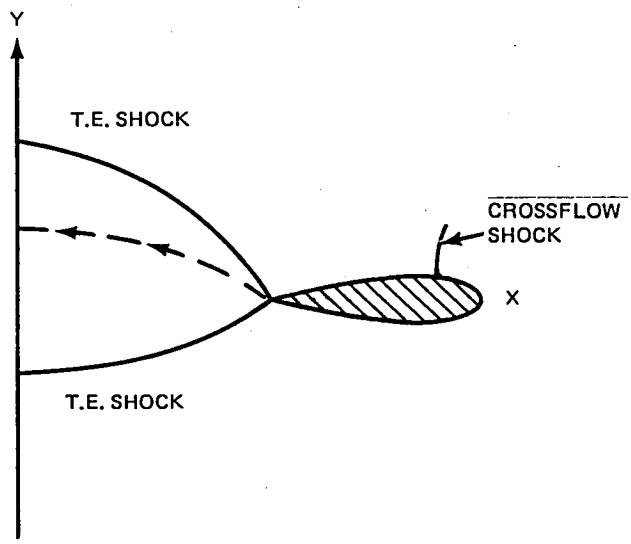


C) SHOCK – EXPANSION ($\alpha > 0$)

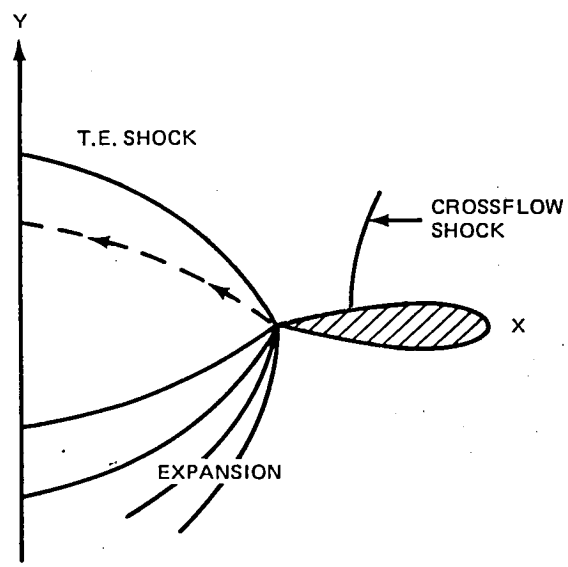


D) SHOCK – EXPANSION ($\alpha > 0$) INTERACTION WITH CROSSFLOW SHOCK

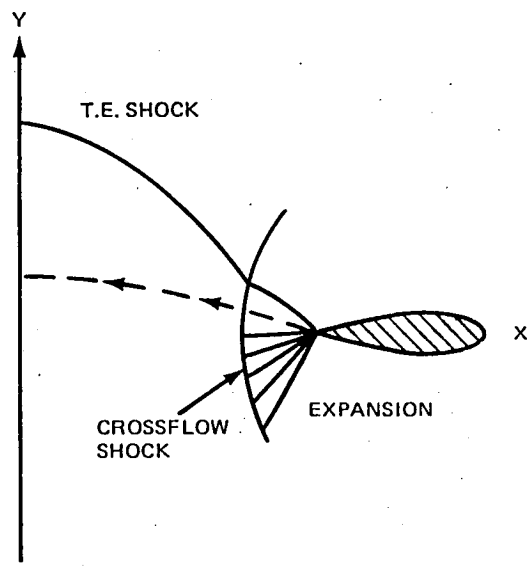


1264-029(T)

**Fig. 23 Sketch of Trailing Edge Shock Interactions (3-D) in the Crossflow Plane**

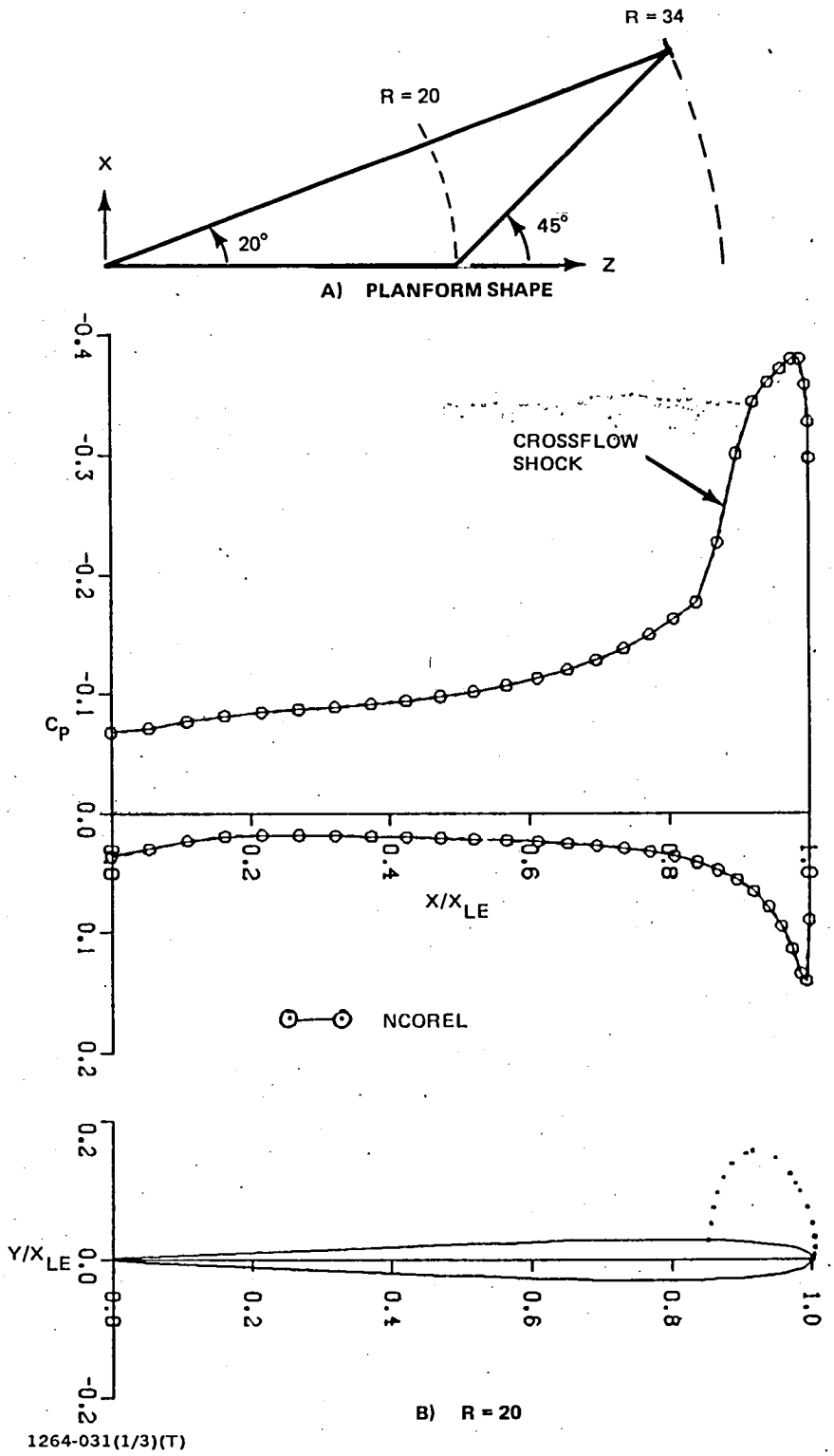


Fig. 24 Sample Arrow Wing Computation at $M_\infty = 1.75$, $\alpha = 5^\circ$ (Sheet 1 of 3)

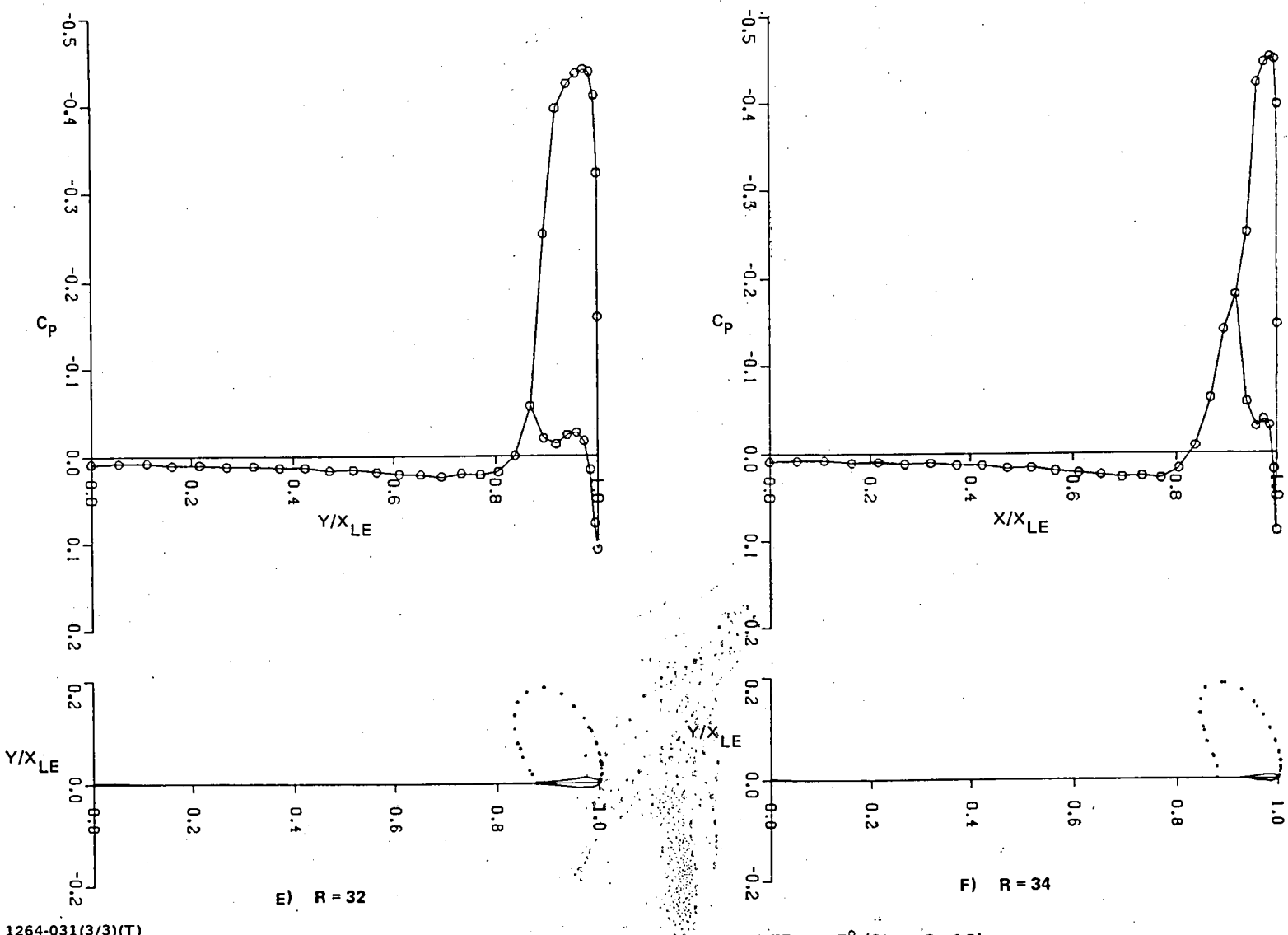


1264-031(3/3)(T)

Fig. 24 Sample Arrow Wing Computation at $M_\infty = 1.75$, $\alpha = 5^\circ$ (Sheet 3 of 3)

trailing edge shock. The lower surface pressures indicate a smooth flow behavior or a very slight expansion. The flat plate solution indicates shocks on both surfaces of the airfoil. Further down the wing, the trailing edge shock becomes somewhat stronger, and the crossflow shock approaches the trailing edge of the wing. Finally, both shocks merge just as the crossflow shock intersects the trailing edge and form a single strong shock at the trailing edge. At the last station, the crossflow shock has passed through the trailing edge shock and exists on the wake cut. The trailing edge solution indicates a shock-expansion behavior at this point. The trailing edge shock, crossflow shock, and expansion interaction are similar to that sketched in Fig. 23d.

Figure 25 indicates a similar behavior at $M_\infty = 1.75$, $\alpha = 10°$ for the same arrow wing. The two shocks merge causing a very strong shock at the trailing edge, and eventually the crossflow shock passes through the trailing edge shock and sits on the wake cut with a shock expansion at the trailing edge. Naturally, this interaction has the built-in approximation of modeling the wake cut as a planar surface. What the effect of fitting the wake exactly would have on these complicated interactions is not known at this point.

The important aspect of modeling the wake properly is to be able to predict the effect of the wake of a lifting surface on a fuselage or other lifting surfaces. To test the wake model, a series of computations were carried out on a set of arrow wings built and tested by NASA Langley (see Ref. 23). Figure 26 shows a sample of the isobar patterns computed, along with the planform shape and centerbody for two of the four models tested at Mach numbers of 2.36, 2.96, and 4.63. Model 1 has a leading edge sweep of 63.4°, and Model 2 was highly swept with a leading edge sweep of 76°. The models were instrumented for pressure, and detailed pressure measurements are available on both the wing and centerbody at flow spanwise sections. One of the spanwise stations was downstream of the centerline trailing edge and serves as a test for the accuracy of the present wake model. One of these wings was computed previously using NCOREL without a wake model, with the result that the body pressures could not be predicted (see Ref. 24). The planform isobar patterns clearly show the crossflow shock on the leeward surface. The crossflow shock intersects the trailing edge wherein the complicated interaction of Fig. 23d takes place. Figure 27 shows a comparison

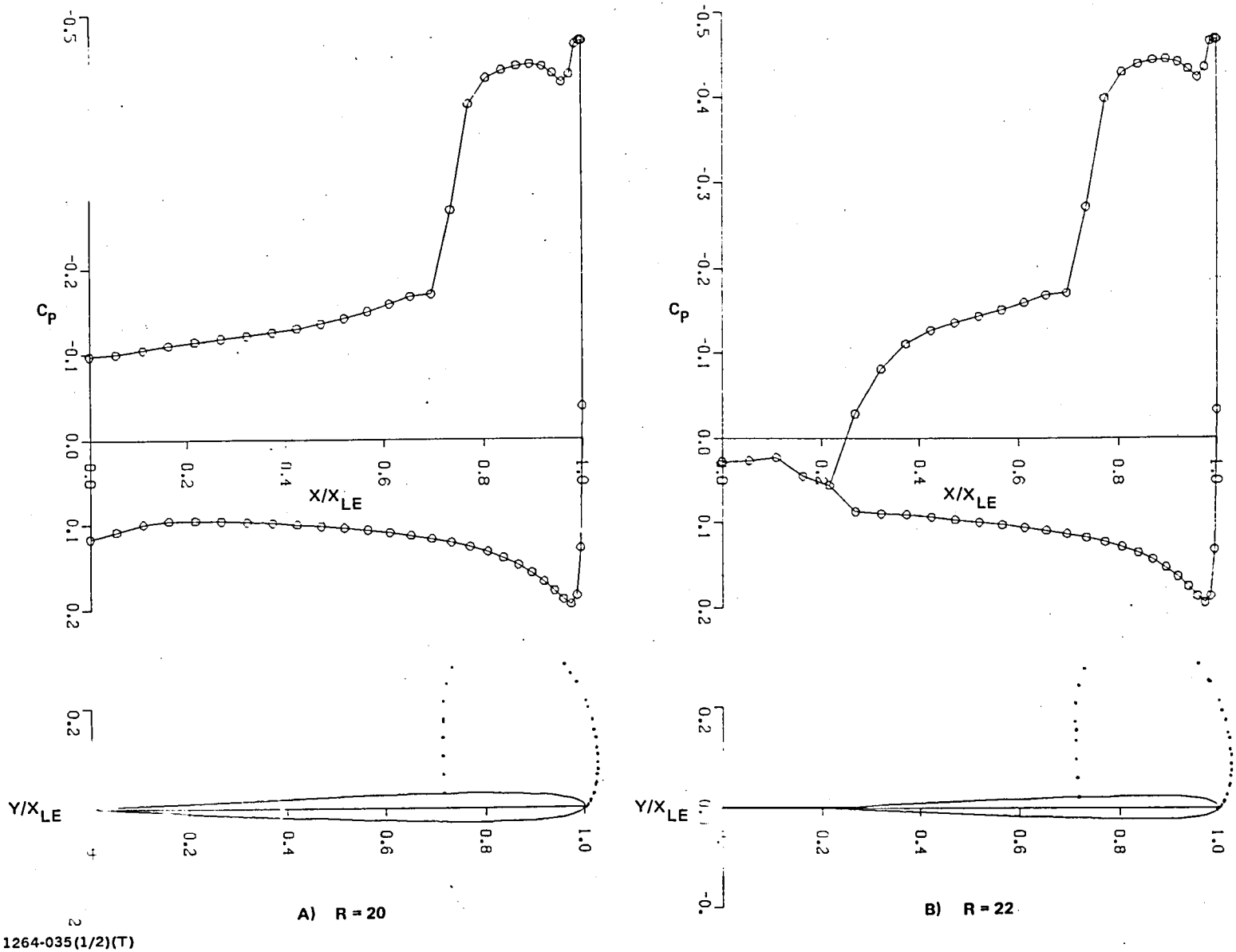


1264-035(1/2)(T)

Fig. 25 Sample Arrow Wing Computation at $M_\infty = 1.75$, $\alpha = 10^\circ$ (Sheet 1 of 2)

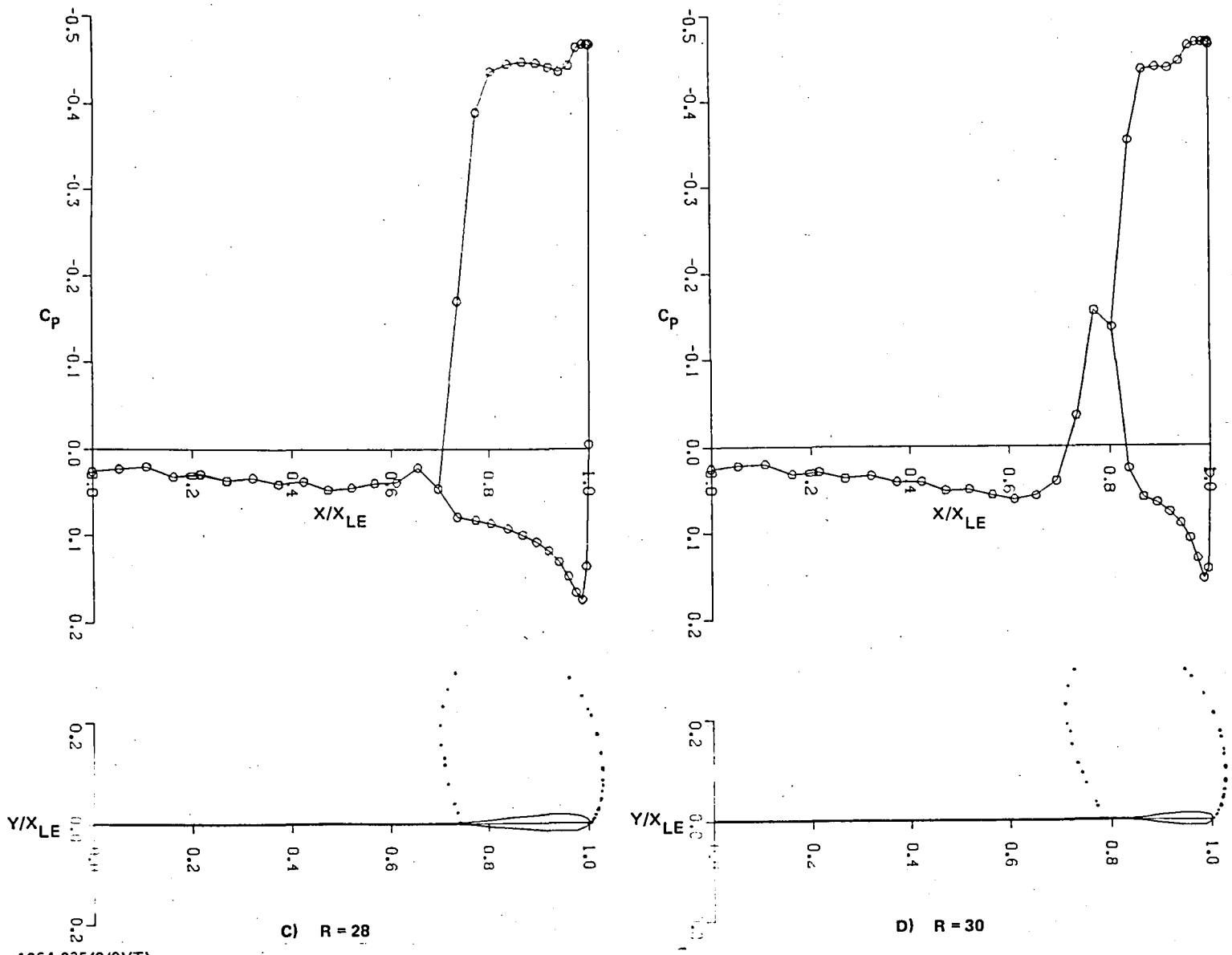


1264-035(2/2)(T)

Fig. 25 Sample Arrow Wing Computation at $M_\infty = 1.75$, $\alpha = 10^\circ$ (Sheet 2 of 2)

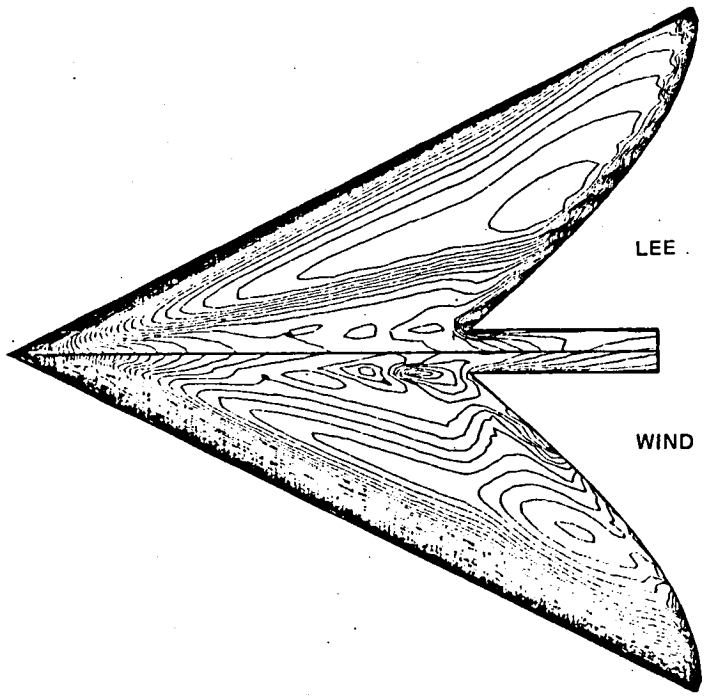


A) MODEL 1 AT $M_\infty = 2.96, \alpha = 6^\circ$

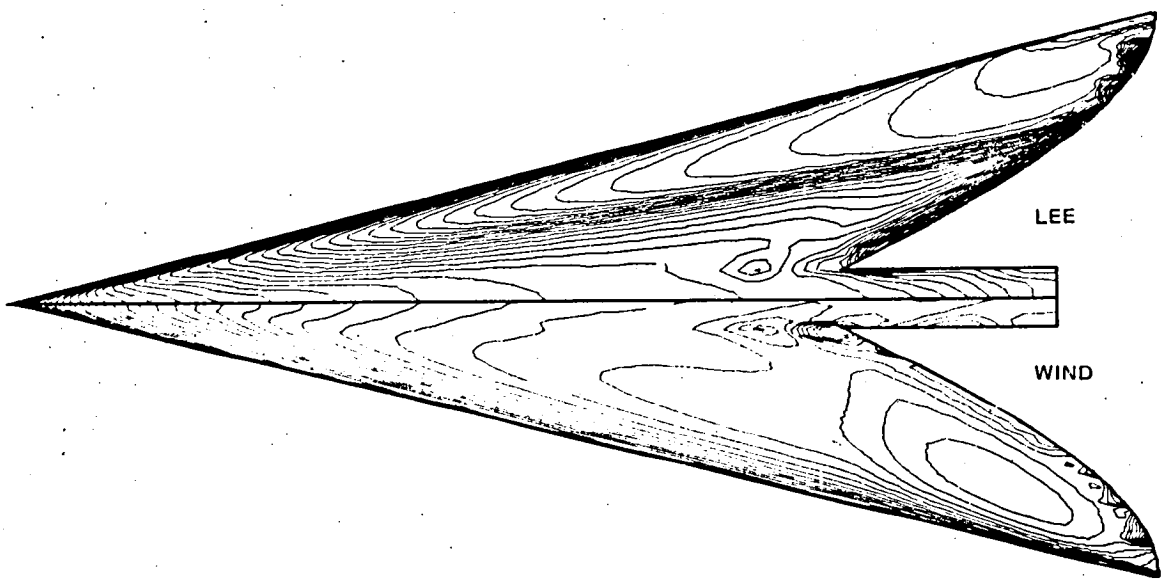


B) MODEL 2 AT $M_\infty = 2.96, \alpha = 6^\circ$

1264-038

Fig. 26 Isobar Planform Pattern for NASA Arrow Wings

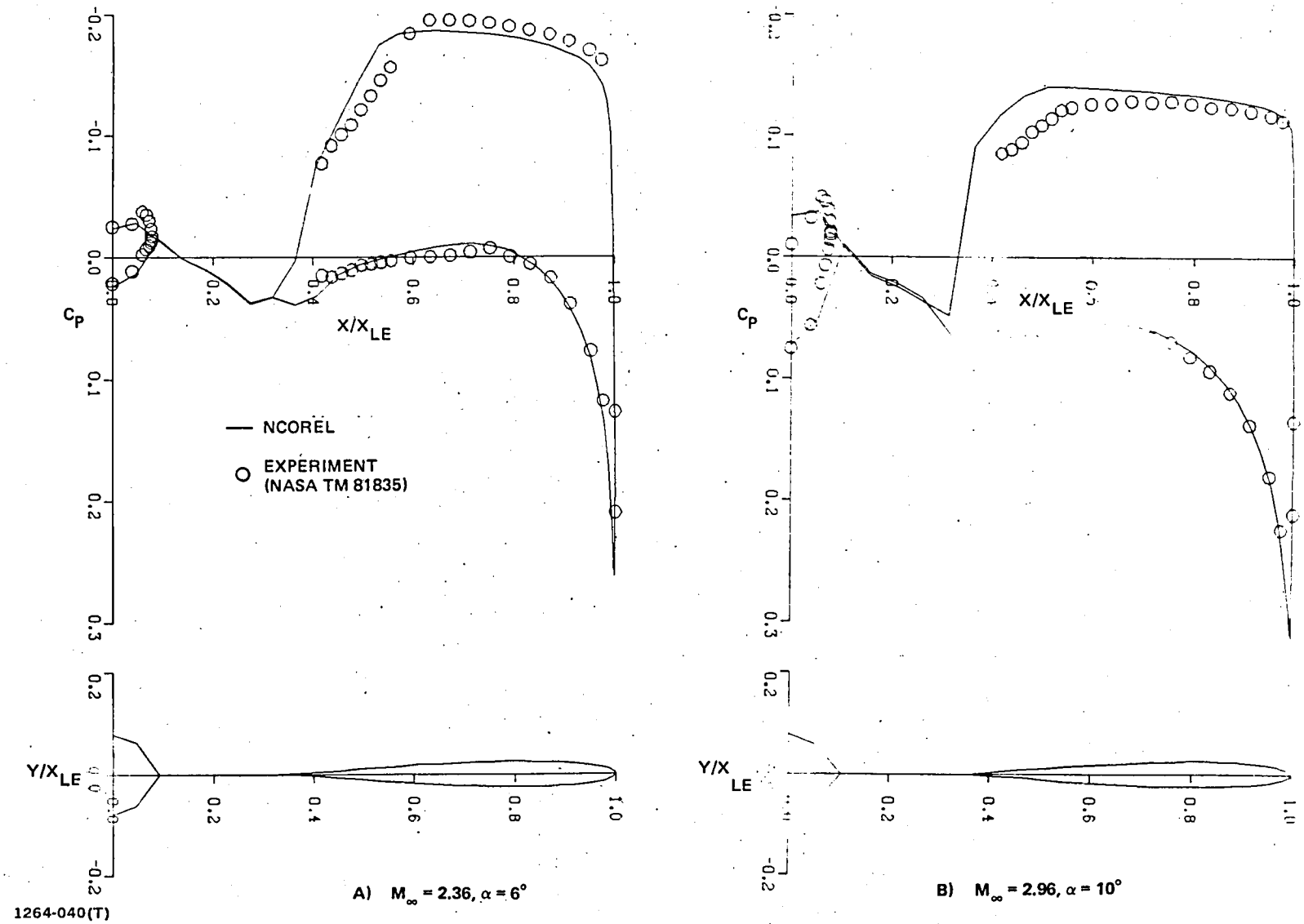


Fig. 27 Model 1 Comparison with Experiment at Spanwise Wake Station

of measured and computed pressures for Model 1 at two different conditions, $M_\infty = 2.36$, $\alpha = 6°$ and $M_\infty = 2.96$, $\alpha = 10°$. Excellent agreement is achieved at the lower Mach number on both the wing and centerbody. At the higher Mach number and incidence, slightly lower pressures are computed in the vicinity of the upper surface trailing edge. Excellent agreement is achieved for the lower wing surface. The body pressures are in good agreement except near the upper surface symmetry plane. Unfortunately, the resolution of the body is quite poor on the mesh that is currently used because the relative size of the body with respect to the wing is quite small for Model 1. Comparisons for the highly swept Model 2 at $\alpha = 3°$ and $6°$ are shown in Fig. 28 and 29 for $M_\infty = 2.36$ and 2.96, respectively. Better resolution of the body is obtained for this model because of its relatively large size in comparison to the wing. Good to excellent agreement is achieved for body pressures. Good agreement is achieved for the lower surface of the wing. Poor correlation is achieved on the upper surface of the wing at the higher incidence. The higher pressure supercritical plateau shown by the measured data at $\alpha = 6°$ is usually indicative of leading edge flow separation and vortex formation and, hence, correlation with computed pressures would not be expected.

### 3.2.2 Arbitrary Cross Sectional Geometries

In general, the wing cross-sectional geometry is not symmetric and can have camber or twist associated with it. If the leading edge is dropped, the placement of the singularity of the conformal wing mapping will generate a grid that will cause a translation of the grid points in the wake cut. Hence, a lower wake cut grid point will not have a corresponding upper wake point. This internal grid generation complicates the implementation of the wake computation. Interpolation of the potential and speed from the lower wake mesh locations into the upper wake must be carried out in order to match the pressures and transverse velocity in the wake cut.

Figure 30 shows a selected sample of the crossflow plane solutions for a cambered arrow wing at $M_\infty = 1.75$, $\alpha = 5°$. This is the same arrow wing as Fig. 24 but with leading edge chordwise droop implemented with a parabolic chordwise camber. Figure 30a shows an early station in the wake. The translation of the upper and lower wake cut points is evident. This becomes increasingly apparent farther downstream in the wake, where twice as many points appear on the wake cut. The interpolation scheme seems to work well for general geometries and has also been implemented for wing-body geometries.

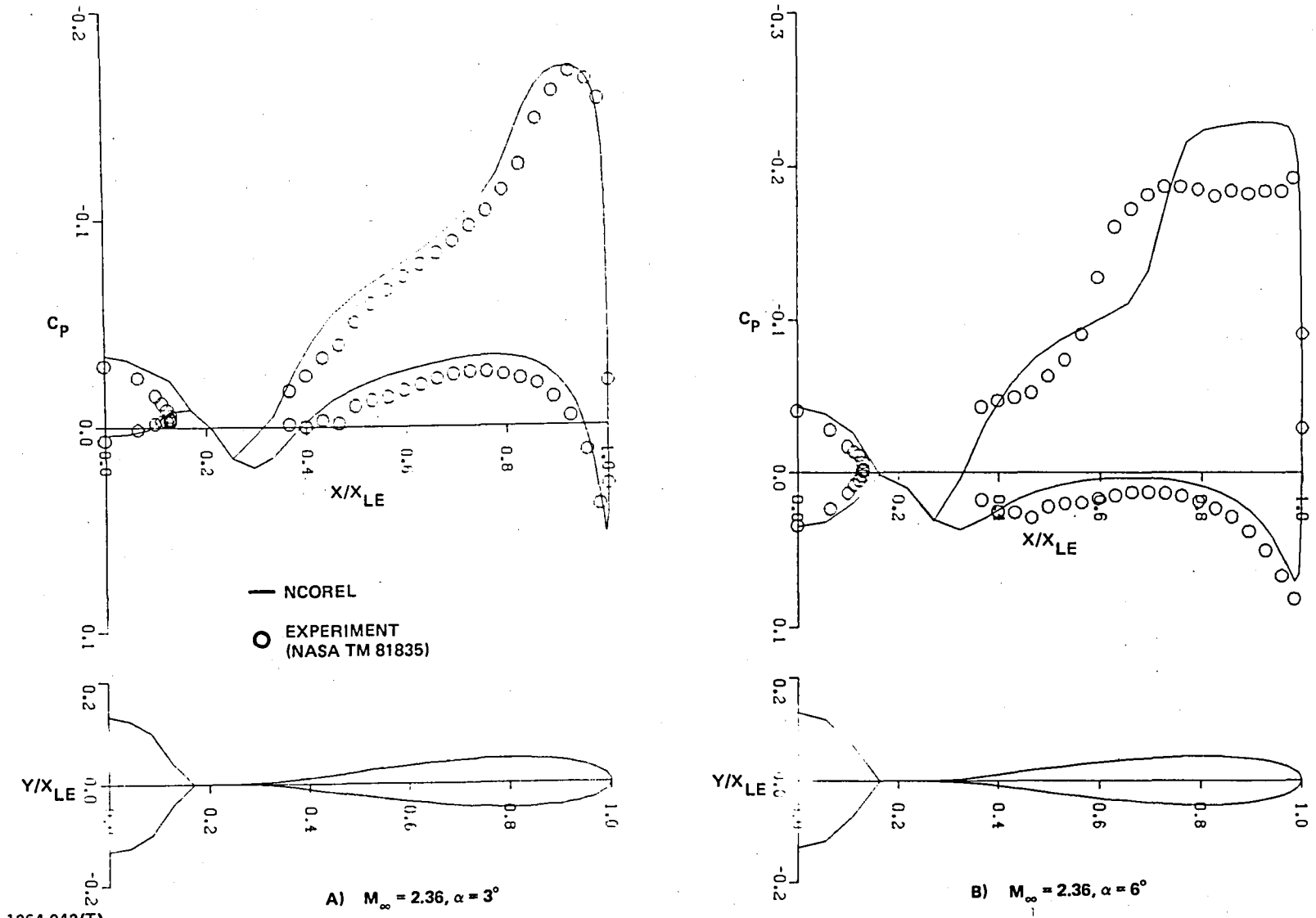


Fig. 28 Model 2 Comparison with Experiment at Spanwise Wake Station

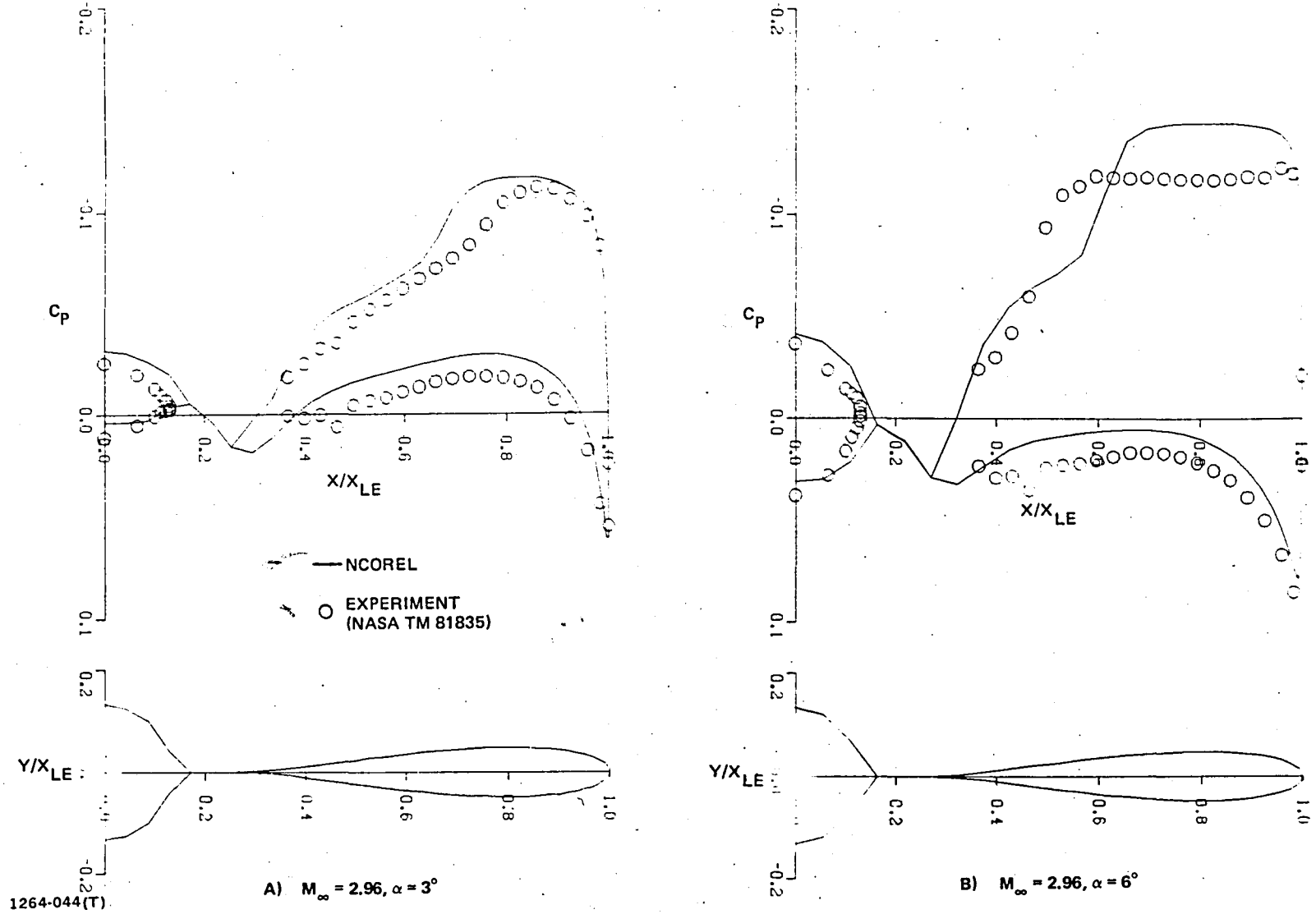


Fig. 29 Model 2 Comparison with Experiment at Spanwise Wake Station

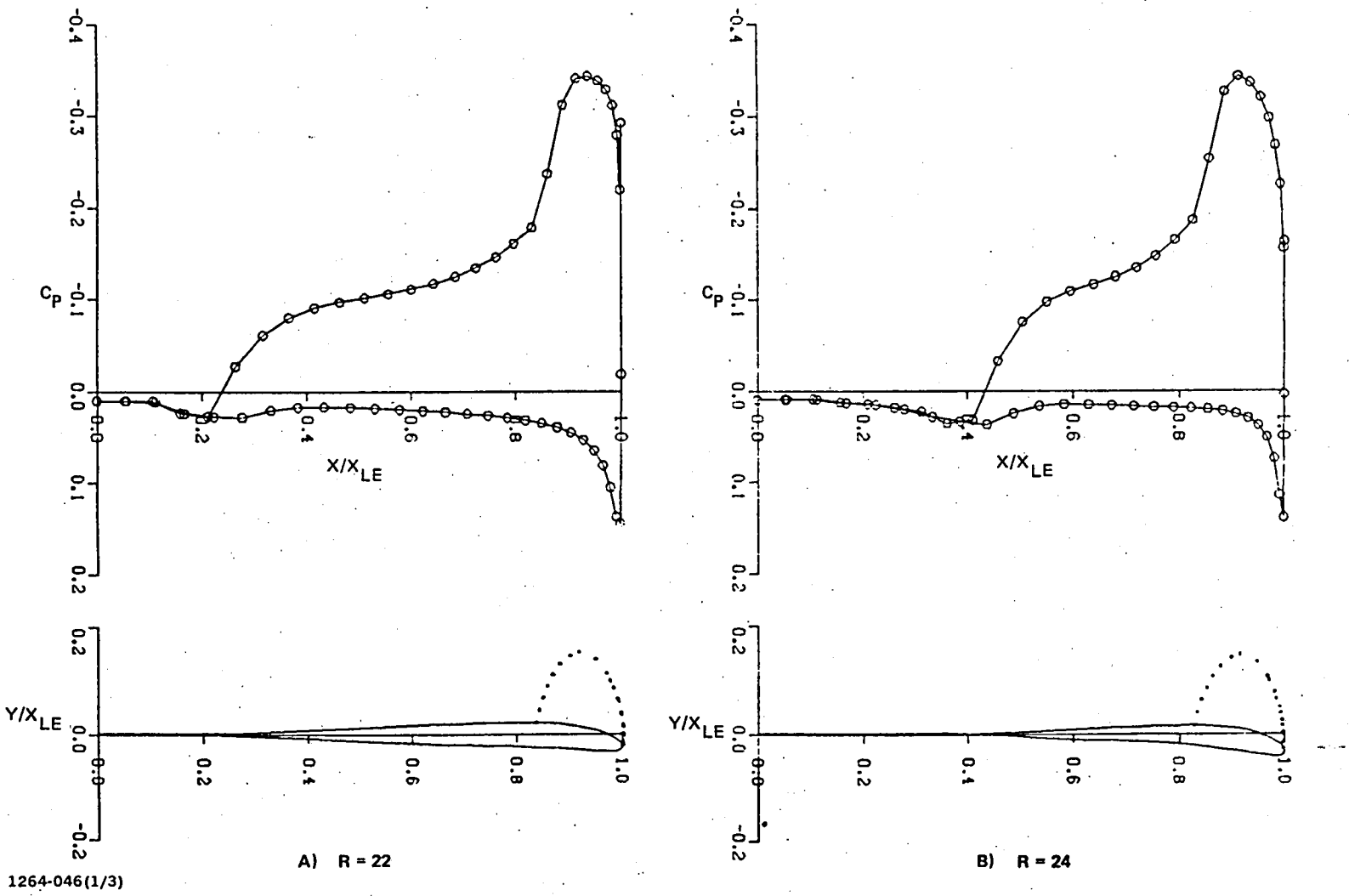


Fig. 30 Cambered Arrow Wing ($\Omega_{LE} = 70°$, $\Omega_{TE} = 45°$) $M_\infty = 1.75$, $\alpha = 5°$ ($C_r = 20$) (Sheet 1 of 3)

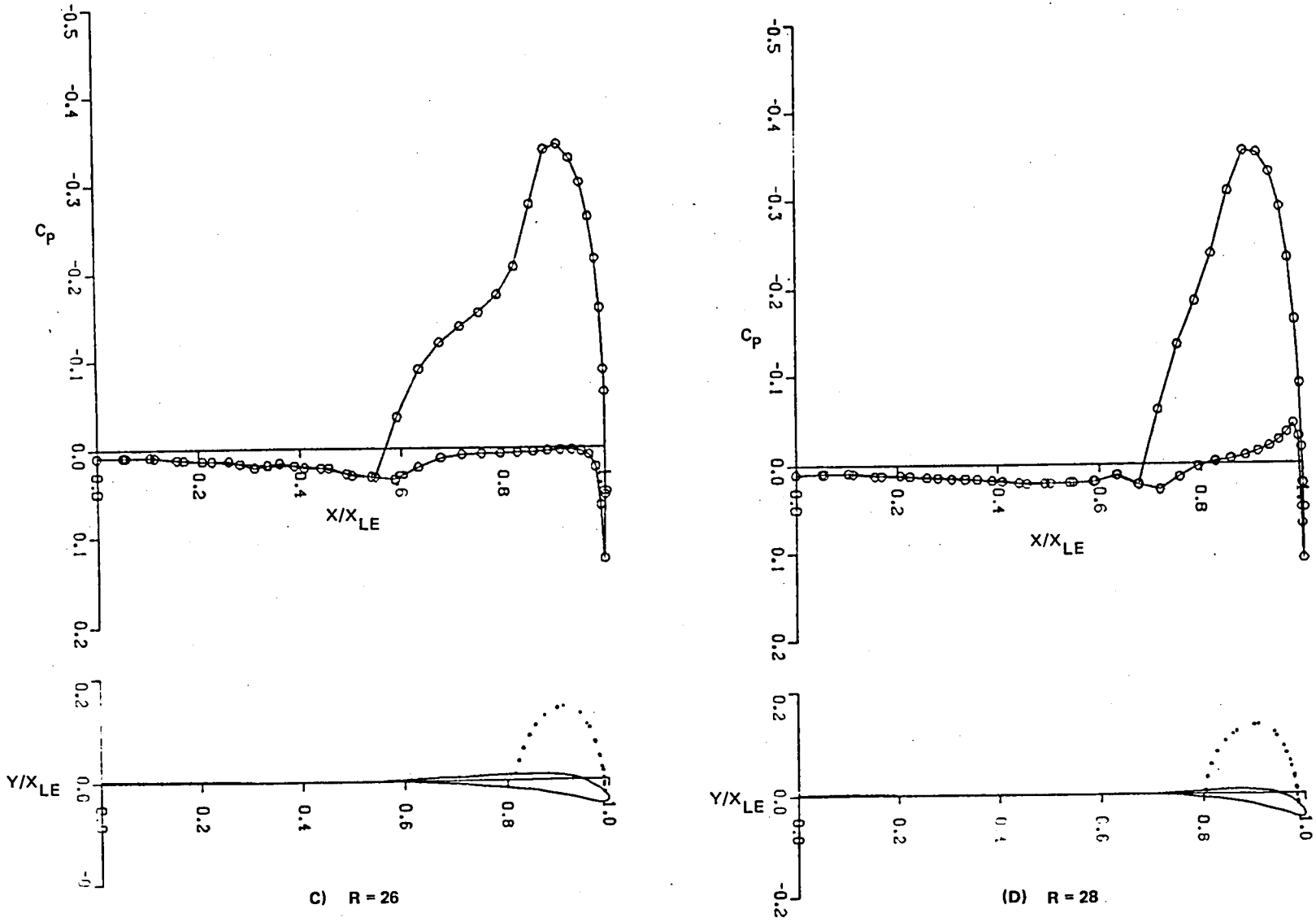


1264-046(2/3)(T)

Fig. 30 Cambered Arrow Wing ($\Omega_{LE} = 70°$, $\Omega_{TE} = 45°$) $M_\infty = 1.75$, $\alpha = 5°$ ($C_r = 20$) (Sheet 2 of 3)

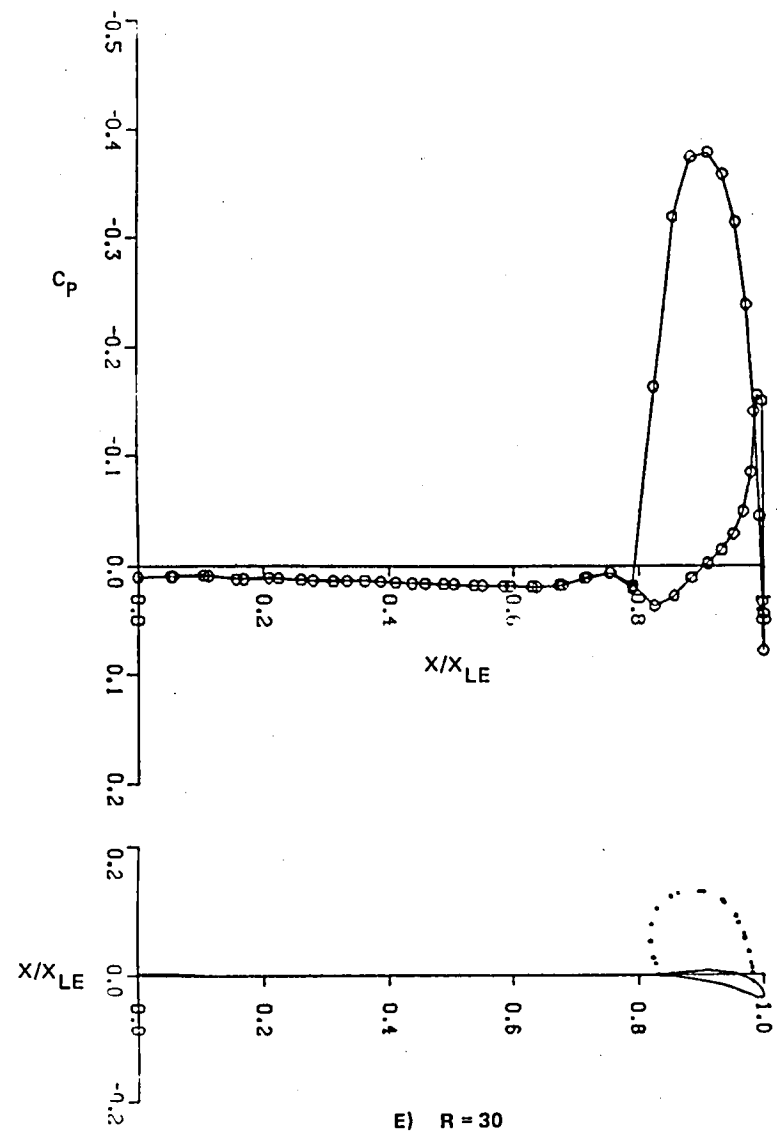


E) R = 30

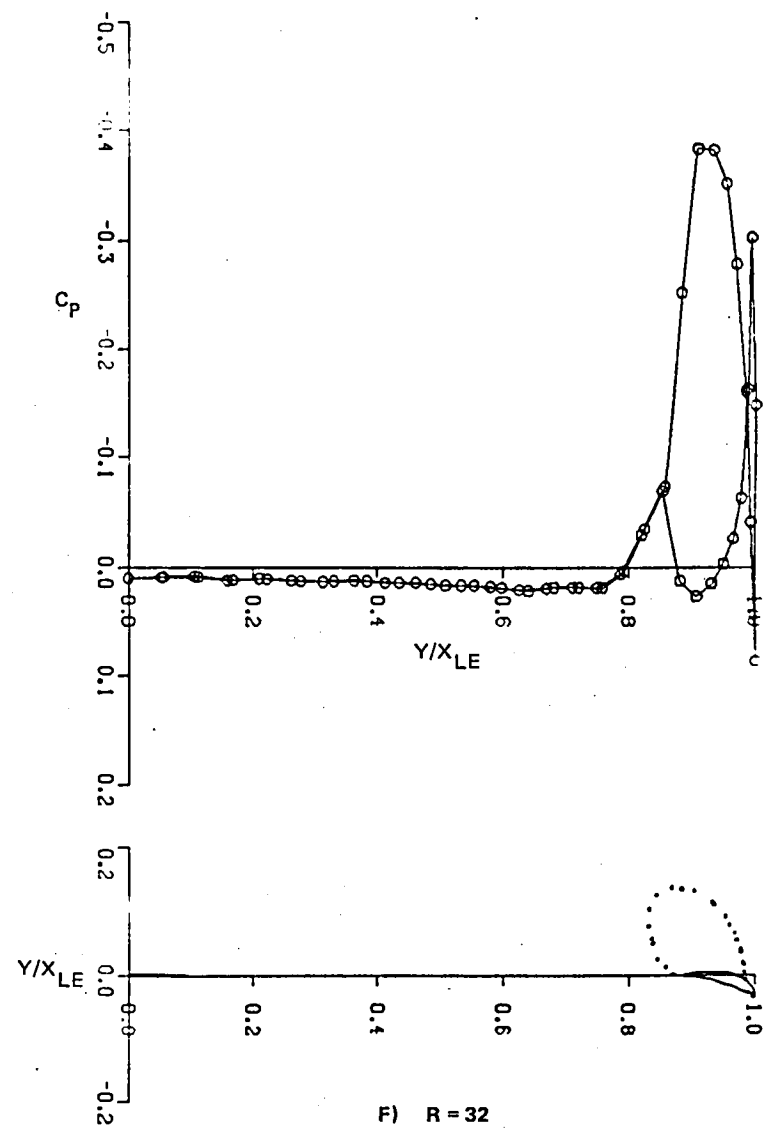


F) R = 32

1264-046(3/3)(T)

Fig. 30 Cambered Arrow Wing ($\Omega_{LE} = 70°$, $\Omega_{TE} = 45°$) $M_\infty = 1.75$, $\alpha = 5°$ ($C_r = 20$) (Sheet 3 of 3)

# 4. CONCLUSIONS

An approximation factorization technique has been successfully applied to the three-dimensional supersonic flow problem. An average overall factor of two reduction in computer time can be expected from the AF1Z scheme.

Supersonic wake flows have also been computed in both conical and three-dimensional full potential flows by modeling the wake as a planar cut with a potential discontinuity. Continuity of pressure was satisfied exactly on the wake cut by computing the necessary potential jump at each wake cut grid point. The conical wake problem is unique in that the jump in potential vanishes in the crossflow symmetry plane. Generally, good correlation was achieved for fully three dimensional wake flows with the planar wake approximation.

## 6. REFERENCES


1. Siclari, M.J., "Investigation of Crossflow Shocks on Delta Wings in Supersonic Flow," AIAA J., Vol 18, No. 1, Jan 1980, p 85.

2. Grossman, B., "Numerical Procedure for the Computation of Irrotational Conical Flows," AIAA J., Vol 17, No. 8, Aug 1979, p 828.

3. Jameson, A., "Iterative Solution of Transonic Flow over Airfoils and Wings, Including Flows at Mach 1," Communication on Pure and Applied Mathematics, Vol 27, May 1974, pp 283-309.

4. Grossman, B. and Siclari, M.J., "Nonlinear Supersonic Potential Flow Over Delta Wings," AIAA J., Vol 19, No. 5, May 1981, p 573.

5. Siclari, M.J., "Supersonic Nonlinear Potential Flow with Implicit Isentropic Shock Fitting," AIAA J., Vol 20, No. 7, July 1982, p 924.

6. Shankar, V., "An Implicit Marching Procedure for the Treatment of Supersonic Flow Fields Using the Conservative Full Potential Equation," AIAA Paper No. 81-1004, presented at AIAA Computational Fluid Dynamics Conf, June 1981.

7. Shankar, V., Osher, S. and Jones, K., "An Efficient Full Potential Implicit Method Based on Characteristics for Analysis of Supersonic Flows," AIAA-82-0974, presented at AIAA/ASME 3rd Joint Thermophysics, Fluids, Plasma and Heat Transfer Conf, June 1982.

8. Sritharan, S.S. and Seebass, A.R., "A Finite Area Method for Nonlinear Conical Flows," AIAA-82-0995, ibid.

9. Bradley, P.F., South, J.C., Dwoyer, D.L., and Keen, J.M., "Vectorized Schemes for Conical Potential Flow using the Artificial Density Method," AIAA 84-0162, presented at AIAA 22nd Aerospace Sciences Mtg, Reno, NV, Jan 1984.

10. Peaceman, D.W. and Rachford, H.H., "The Numerical Solution of Parabolic and Elliptic Differential Equations," J. Soc Indust Ap Mech, Vol 3, 1955, pp 28-41.

11. Ballhaus, W.F., Jameson, A. and Albert, J., "Implicit Approximate Factorization Schemes for the Efficient Solution of Steady Transonic Flow Problems," AIAA J., Vol 16, June 1978, pp 573-579.

12. Holst, T.L., "Fast, Conservative Algorithm for Solving the Transonic Full-Potential Equation," AIAA J., Vol 18, No. 12, Dec 1980, pp 1431-1439.

13. Baker, T.J., "A Fast Implicit Algorithm for the Nonconservative Potential Equation," Open Forum Presentation at AIAA 4th Computational Fluid Dynamics Conf, July 1979.

14. Baker, T.J., "Potential Flow Calculation by the Approximate Factorization Method," J. of Comp Physics, 42, 1-19 (1981).

15. Catherall, D., "Optimum Approximate-Factorization Schemes for 2D Steady Potential Flows," AIAA Paper No. 81-1018, presented at AIAA Computational Fluid Dynamics Conf, June 1981.

16. Jameson, A., "Acceleration of Transonic Potential Flow Calculations on Arbitrary Meshes by the Multiple Grid Method," AIAA paper No. 79-1458, presented at AIAA Computational Fluid Dynamics Conf, July 1979.

17. Siclari, M.J., "Approximate Factorization Schemes for 3D Nonlinear Supersonic Potential Flow," AIAA-83-0376, presented at AIAA 21st Aerospace Sciences Mtg, Reno, NV, Jan 1983.

18. Siclari, M.J., "The NCOREL Computer Program for 3D Nonlinear Supersonic Potential Flow Computations," NASA CR 3694, Contract NAS1-16758, Aug 1983.

19. Pittman, J.L., Miller, D.S. and Mason, W.H., "Supersonic, Attached-Flow Wing Design for High Lift with Experimental Validation," NASA TP-2336, Aug 1984.

20. Mangler, K.W., and Smith, J.H.B., "Behavior of the Vortex Sheet at the Trailing Edge of a Lifting Wing," The Aeronautical J. of the Royal Aeronautical Soc, Vol 74, Nov 1970, pp 906-908.

21. Shankar, V. and Szema, K.Y., "A Conservative Type-Dependent Full Potential Method for the Treatment of Supersonic Flows with Embedded Subsonic Regions," AIAA Paper No. 83-1887, presented at AIAA Computational Fluid Dynamics Conf, Danvers, MA, July 1983.

22. Smith, J.H.B., "Remarks on the Structure of Conical Flow," Progress in Aeronautical Sciences, Vol 12, 1972, pp 241-271.

23. Townsend, J.C., "Pressure Data for Four Analytically Defined Arrow Wings in Supersonic Flow," NASA TM-81835, Sept 1980.

24. Siclari, M.J., "Computation of Nonlinear Supersonic Potential Flow Over Three-Dimensional Surfaces," J. of Aircraft, Vol 20, No. 5, May 1983, p 462.

**APPENDIX A:** NCOREL
PHASE II VERSION
USER'S MANUAL UPDATE
(NASA CR-3694)

**NOTE:** The following variables have been added to the NAMELIST input. Section VIII summarizes all of the additional namelist inputs.

## I. Approximate Factorization Scheme (AF1Z)

An AF1 scheme has been added to NCOREL for both bow shock capture and fit options. This scheme can reduce the computer time by a factor of two to three.

| Namelist Variable | Description |
|---|---|
| IAF<br>IAF = 0 (SLOR)<br>IAF = 1 (AF1Z) | Optional switch for relaxation scheme |

| Conical Control Parameters | Description |
|---|---|
| NCYC(K), K=1, KREF<br>AFMIN(K), "<br>AFMAX(K), "<br>NCYC = 3 or 4<br>AFMIN = .5<br>AFMAX = 2.0 | NCYC is the number of cycles from the maximum to minimum acceleration parameter.<br><br>High Mach (i.e., > $M_\infty$ = 2.5) starts for bow shock fitting on crude grids may require 6-8 cycles and AFMIN = 3, AFMAX = 6. Sensitivity mostly to AFMIN. |

| Nonconical Control Parameters | |
|---|---|
| NCYCR<br>AFMINR<br>AFMAXR | These parameters treated similar to conical parameters. |

**Important:** The AF1Z is sensitive to the temporal damping parameter (EST). Small values of EST (i.e., -.01 or -.001) should be used or convergence will deteriorate dramatically.

## II. Crossflow Y-Stretching

| | |
|---|---|
| NPOW<br><br>NPOW = 0 EVEN<br>NPOW = 1 Clustered toward body | Two types of crossflow radial meshes are available.<br>NPOW = 0, evenly spaced radial mesh;<br>NPOW = 1, hyperbolic stretching which clusters grid points near the body surface. |

## III. Bow Shock Fitting Parameters

IENTRY

The code will fit the bow shock isentropically or with the Rankine-Hugoniot shock conditions. With the Rankine-Hugoniot shock, the flow field pressures are corrected by the computed bow shock entropy.

IENTRY = 0 — Isentropic bow shock
IENTRY = 1 — Rankine-Hugoniot bow shock

ITSHKC
ITSHKR

The number of initial iterations for which the bow shock conditions are held fixed before updating.
ITSHKC, conical
ITSHKR, nonconical

ITSHKC = 0 to 15
ITSHKR = 0 to 5

IBOW

An additional option has been included to implicitly fit the bow shock in 3D. This option yields a fully second order bow shock computation.

IBOW = 1 — First order bow shock. Marching meshes held fixed.

IBOW = 2 — Second order implicit bow shock. 3D mesh position updated in a similar fashion to conical.

**Important:** IBOW = 2 will significantly increase the computing time by a factor of two to three. In addition, it should only be used at high Mach (i.e., $M_\infty > 2.5$). Can eliminate first order marching instability at high Mach number using large step sizes. The 3D bow shock relaxation parameter (RELNC) must be reduced to near conical values for IBOW = 2.

ISMOO

Bow Shock Angle Smoothing. This option should only be used as last resort if bow shock instability arises at high Mach number.

Can be used with IBOW=1 or IBOW=2.

ISMOO = 0 — No smoothing.
ISMOO = 1 — Smoothing.

## IV. Geometry Interpolation

| | |
|---|---|
| ILIN | Optional mapped space body shape interpolation. |
| ILIN = 0 | Linear Interpolation. Should be used when cross sections have abrupt changes. For example, unfaired wing-body cross sections or nearly rectangular body shapes. The cubic spline fitting can produce unpredictable results. The maximum number of geometry points (e.g., 99) should be used with IL1N = 0. |
| IL1N = 1 | Cubic spline fitting. |

## V. Supersonic Crossflow Region

| | |
|---|---|
| ISUP | |
| ISUP = 1 | First order accurate treatment of supersonic crossflow points. |
| ISUP = 2 | Second order accurate treatment of supersonic crossflow points. |

## VI. Wake Computation

| | |
|---|---|
| IWAKE | |
| IWAKE = 0 | Wake cut treated as impermeable flat plate |
| IWAKE = 1 | Turns on wake computation. Wake should be modeled as smooth extension of trailing edge. |
| IBODY | Only used if IWAKE $\neq$ 0 |
| IBODY = 0 | Wing alone |
| IBODY = 1 | Wing-body configuration |

**Note:** If IBODY = 1, a subroutine BODYW must be included that yields the maximum width of the body at a given axial location.

| | |
|---|---|
| RELWK | Relaxation factor for wake pressure match |

$.25 < RELWK < 1.0$

## VII. Other Namelist Parameters

| | |
|---|---|
| DMINR<br>1.E-4 < DMINR < 1.E-2 | Maximum residual tolerance for convergence at nonconical stations. |
| OMEGR<br><br>1.5 < OMEGR < 1.7 | Relaxation parameter for potential at nonconical stations. |

## VIII. Summary of Additional Namelist Parameters

| | |
|---|---|
| 1. Approximate Factorization | IAF<br>NCYC(K),AFMIN(K),AFMAX(K), K=1,3<br>NCYCR, AFMINR, AFMAXR |
| 2. Grid Control | NPOW |
| 3. Bow Shock Fitting | IBOW<br>IENTRY<br>ITSHKC<br>ITSHKR<br>ISMOO |
| 4. Geometry Interpolation | ILIN |
| 5. Supersonic Crossflow | ISUP |
| 6. Wake Computation | IWAKE<br>IBODY<br>RELWK |
| 7. Other | DMINR<br>OMEGR |

| 1. Report No. | 2. Government Accession No. | 3. Recipient's Catalog No. |
|---|---|---|
| NASA CR-172456 | | |

| 4. Title and Subtitle | 5. Report Date |
|---|---|
| SUPERSONIC NONLINEAR POTENTIAL FLOW ANALYSIS - INTERIM REPORT | August 1984 |
| | 6. Performing Organization Code |
| 7. Author(s) | 8. Performing Organization Report No. |
| Michael J. Siclari | RE-690 |
| 9. Performing Organization Name and Address | 10. Work Unit No. |
| Grumman Aerospace Corporation<br>Research and Development Center<br>Bethpage, New York 11714 | 11. Contract or Grant No.<br>NAS1-16758 |
| 12. Sponsoring Agency Name and Address | 13. Type of Report and Period Covered |
| National Aeronautics and Space Administration<br>Washington, D.C. 20546 | Contractor Report |
| | 14. Sponsoring Agency Code<br>505-43-23-03 |

15. Supplementary Notes

Langley Technical Monitors: James Pittman and David S. Miller
Interim Report

16. Abstract

NCOREL is a computer code that has been established to numerically compute supersonic flow fields about wings and bodies. The method encompasses an implicit finite difference transonic relaxation method for solving the full potential equation in a spherical coordinate system. In the present work, two basic topics are studied with the aim of broadening the applicability and usefulness of the present method encompassed within the computer code NCOREL for the treatment of supersonic flow problems. The first topic is that of computing efficiency. Accelerated schemes exist and are in current use for transonic flow problems. One such scheme is the approximate factorization (AF) method. This study will develop and apply an AF scheme to the supersonic flow problem. The second topic that will be addressed will be the computation of wake flows. The proper modeling of wake flows is important for multi-component configurations such as wing-body and multiple lifting surfaces where the wake of one lifting surface will have a pronounced effect on a downstream body or other lifting surface.

| 17. Key Words (Suggested by Author(s)) | 18. Distribution Statement |
|---|---|
| Supersonic Flow<br>Nonlinear Potential Flow<br>NCOREL | Unclassified - Unlimited<br><br>Subject Category 02 |

| 19. Security Classif. (of this report) | 20. Security Classif. (of this page) | 21. No. of Pages | 22. Price |
|---|---|---|---|
| Unclassified | Unclassified | 81 | A05 |



For sale by the National Technical Information Service, Springfield, Virginia 22161